



universität
wien

MASTERARBEIT / MASTER'S THESIS

Titel der Masterarbeit / Title of the Master's Thesis

Functional analysis of the polymorphic tandem repeats
minisatellite MNS16A of human telomerase gene in
prostate and lung cancer cell lines

verfasst von / submitted by

Christian Behm, BSc

angestrebter akademischer Grad / in partial fulfilment of the requirements for the degree of
Master of Science (MSc)

Wien, 2015 / Vienna 2015

Studienkennzahl lt. Studienblatt /
degree programme code as it appears on
the student record sheet:

A 066 834

Studienrichtung lt. Studienblatt /
degree programme as it appears on
the student record sheet:

Masterstudium Molekulare Biologie UG2002

Betreut von / Supervisor:

Ao. Univ.-Prof. Mag. Dr. Andrea Gsur

Danksagung

Ein herzliches Dankeschön gebührt meiner Betreuerin Frau Ao. Univ.-Prof. Mag. Dr. Andrea Gsur (Institut für Krebsforschung, Klinik für Innere Medizin 1, Medizinische Universität Wien), die diese Arbeit erst ermöglicht hat. Danke für die Betreuung und Beurteilung meiner Arbeit.

Ein großer Dank gebührt auch Frau Assoc. Prof. Priv.-Doz. Mag. Dr. Hedwig Sutterlüty-Fall (Institut für Krebsforschung, Klinik für Innere Medizin 1, Medizinische Universität Wien), die die Gerätschaften für diese Arbeit zur Verfügung gestellt hat. Danke, dass Sie mir in Hinblick auf die Arbeitsmethoden immer mit Rat und Tat zur Seite standen.

Weiters möchte ich mich bei Herrn Mag. Dr. Andreas Baierl (Department of Statistics and Decision Support Systems, Universität Wien) für die Unterstützung bei der statistischen Auswertung meiner Ergebnisse bedanken.

Dankeschön auch an alle „Gsurlis“: Philipp, Stefanie, Cornelia und Elisabeth. Danke für die vielen lehrreichen und vor allem lustigen Gespräche im Labor und für ein wirklich sehr gutes Arbeitsklima.

Ein großes Dankeschön geht auch an Angelina, Vanita, Rosana und Jihen. Vielen herzlichen Dank, dass ihr mich so problemlos in euren Laboralltag integriert und mich in den unterschiedlichen Arbeitsmethoden unterwiesen habt. Danke auch für die zahlreichen freundschaftlichen Gespräche.

Mein größter Dank gilt aber meiner Familie, allen voran meiner besten Freundin und Lebenspartnerin Verena Ferstl. Danke für deine bedingungslose Liebe und Unterstützung während des gesamten Studiums. Dein Zusprechen und deine aufmunternden Worte haben mir sehr viel Kraft gegeben diesen Lebensabschnitt zu meistern. Danke schön.

Ein großer Dank natürlich auch an meine Eltern, Gerlinde und Ernst Behm, sowie an meinen Bruder Thomas Behm und meine Großeltern, Josepha und Friedrich Gabriel. Danke, dass ihr mich immer uneingeschränkt unterstützt habt. Ohne euch wäre dieses Studium überhaupt nicht möglich gewesen.

Vielen herzlichen Dank an Gertrude, Eduard und Tanja Ferstl. Ein großes Dankeschön auch an Jennifer Ferstl, die uns mit ihrer heiteren Persönlichkeit so manchen lustigen Moment beschert hat.

Abstract

MNS16A, a polymorphic tandem repeats minisatellite in the promoter region of the antisense transcript of the human telomerase reverse transcriptase (hTERT) gene, has been discussed as a biomarker in several malignancies.

The present master thesis investigated, for the first time, the functionality of all six known MNS16A VNTRs in the lung cancer cell line A-427 and the prostate cancer cell line LNCaP, using a Dual-Luciferase reporter assay system.

All six MNS16A VNTRs showed statistically significant promoter activity in both cancer cell lines. LNCaP exhibited a statistically significant increase of promoter activity with decreasing MNS16A length for all six considered VNTRs, reflecting a strong negative linear relationship ($p=0.00078$) in the prostate cancer cell line. However, this trend was not observed in A-427. In A-427, VNTR-364, the longest allele, showed the lowest promoter activity, however no significant differences between the remaining five VNTRs were observed.

These results suggest that MNS16A functionality might differ in different cancer cell types and may not follow a linear function in all cell lines as observed in LNCaP. Further studies are warranted to investigate MNS16A functionality in additional prostate and lung cancer cell lines and in various other cancer cell lines.

Kurzfassung

Der polymorphe Minisatellit MNS16A befindet sich downstream des humanen Telomerase Reverse Transcriptase (hTERT) Gens, in der Promoterregion des antisense hTERT Transkriptes. MNS16A wurde in zahlreichen molekular-epidemiologischen Studien als möglicher Biomarker für unterschiedliche Krebserkrankungen untersucht. Im Zuge dieser Studien wurden bisher sechs verschiedene Varianten mit einer variablen Anzahl an Tandemwiederholungen (VNTRs) von MNS16A identifiziert.

Ziel der vorliegenden Masterarbeit war, zum ersten Mal, der Funktionalitätsnachweis aller sechs bekannten MNS16A Varianten, nicht nur in der Lungenkrebs-Zelllinie A-427, sondern auch in der Prostatakrebs-Zelllinie LNCaP, unter Verwendung eines Dual-Luciferase Reporter Systems.

Alle sechs MNS16A VNTRs zeigten eine statistisch signifikante Promoteraktivität in beiden Krebszelllinien. In der Prostatakrebs-Zelllinie zeigte sich eine statistisch signifikante Zunahme der Promoteraktivität mit abnehmender MNS16A Länge. Dies deutet auf ein starkes negatives lineares Verhältnis ($p=0.00078$) in der Prostatakrebs-Zelllinie hin. Allerdings konnte dieses Verhältnis in die Lungenkrebs-Zelllinie A-427 nicht bestätigt werden. Obwohl in A-427 das längste Allel eine deutlich geringere Promoteraktivität aufweist als die übrigen MNS16A Varianten, gelang es nicht, einen statistisch signifikanten Unterschied in der Aktivität der kürzeren Allele nachzuweisen.

Diese Resultate weisen auf ein unterschiedliches Verhalten von MNS16A in unterschiedlichen Krebszellen hin. Weitere Studien, die die MNS16A Funktionalität in zusätzlichen Lungen- und Prostatakrebs-Zelllinien und in anderen Krebszelllinien untersuchen, können zur weiteren Aufklärung der MNS16A Funktionalität beitragen.

Table of contents

Danksagung	I
Abstract.....	III
Kurzfassung.....	V
Abbreviations	IX
1. Introduction	1
1.1. Prostate cancer	1
1.1.1. Epidemiology of prostate cancer	1
1.1.1. Molecular epidemiology of prostate cancer	1
1.2. Lung cancer.....	2
1.2.1. Epidemiology of lung cancer	2
1.2.2. Histology of lung cancer	3
1.2.3. Molecular epidemiology of lung cancer.....	3
1.3. Telomeres and telomerase.....	4
1.3.1. Telomere structure and function	4
1.3.2. Telomerase and the hTERT gene	5
1.3.2.1. Telomerase structure and function	5
1.3.2.2. The hTERT gene	5
1.3.2.3. Telomerase activity regulation	5
1.3.3. Role of telomere and telomerase in tumorigenesis	6
1.3.3.1. Telomere shortening and carcinogenesis.....	6
1.3.3.2. Telomerase activity in tumorigenesis	7
1.3.3.3. Telomere length and cancer	7
1.3.3.4. Association between hTERT locus genetic variants and cancer risk	8
1.4. MNS16A	9
2. Aim of the study	11
3. Materials and methods.....	12
3.1. Molecular biology	12
3.1.1. Cloning	12
3.1.1.1. Restrictiondigests.....	12
3.1.1.2. Agarosegelelektrophorese	14
3.1.1.3. DNA fragment extraction from gel	15
3.1.1.4. Ligation.....	16
3.1.1.5. E. Coli transformation	16

3.1.1.6.	STETL (Sucrose-Triton-EDTA-HCl-Lysozyme) mini-preparation.....	17
3.1.2.	DNA purification by cesium chloride banding	18
3.2.	Cell biology.....	21
3.2.1.	Cell lines.....	21
3.2.2.	Cell cultivation	21
3.2.3.	Calcium phosphate transfection	22
3.2.3.1.	CFP-DNA transfection	22
3.2.3.2.	MNS16A VNTRs transfection	23
3.2.4.	Determination of transfection efficiency.....	24
3.2.5.	Dual-Luciferase reporter assay.....	25
3.3.	Statistical evaluation	26
3.3.1.	MNS16A functional analysis	26
4.	Results.....	27
4.1.	Preparatory experiments	27
4.1.1.	Cloning MNS16A alleles	27
4.1.2.	DNA purification by cesium chloride banding	28
4.1.2.1.	First cesium chloride preparation of cloned MNS16A constructs	28
4.1.2.2.	Second cesium chloride preparation of cloned MNS16A constructs	31
4.2.	Qualitative determination of transfection efficiency of cell lines.....	33
4.2.1.	Lung cancer cell lines.....	33
4.2.2.	Prostate cancer cell lines	34
4.3.	MNS16A functional analysis.....	37
4.3.1.	MNS16A promoter activity in A-427	37
4.3.2.	MNS16A promoter activity in LNCaP.....	39
4.3.3.	A-427 MNS16A promoter activity compared to LNCaP.....	41
5.	Discussion	42
	References.....	50
	List of figures.....	58
	List of tables.....	59
	Appendix 1: MNS16A allele sequences	60
	Appendix 2: Vector maps.....	61
	Appendix 3: Abstract.....	67
	Appendix 4: Kurzfassung.....	68
	Curriculum Vitae	70

Abbreviations

Amp	Ampicillin
ATCC	American Type Culture Collection
BAT3	BCL2-associated athanogene 6 gene
BBS	BES buffered solution
Bp	Base pair
BPH	Benign prostatic hyperplasia
BSA	Bovine serum albumin
CFP	Cyan fluorescent protein
CMV	Cytomegalovirus
CRC	Colorectal cancer
Df	Degrees of freedom
DKC1	dyskerin gene, coding for: H/ACA ribonucleoprotein complex subunit 4
DMEM	Dulbecco's modified eagle's medium
DMSO	Dimethylsulfoxid
DNA	Desoxyribonucleic acid
DTE	Dithioerythritol
DTT	Dithiothreitol
E.coli	Escherichia Coli
EDTA	Ethylenediaminetetraacetate
FCS	Fetal calf serum
GATA	GATA binding factor
GATA-1	Erythroid transcription factor
GBM	Glioblastoma mutliforme
GWAS	Genome wide association studies
HBS	HEPES bufferes saline
HIV	Human immunodeficiency virus
hTERT	Human telomerase reverse transcriptase gene/protein
hTR	Human telomerase RNA component gene/protein
ICR	Institute of Cancer Research, Medical University of Vienna
miRNA	Micro RNA

Ms	Milliseconds
MSMB	Beta-microseminoprotein gene
MYC	Myelocytomatosis oncogene
nAChR	nicotine acetylcholine receptor subunit gene
NHP2	H/ACA ribonucleoprotein complex subunit 2
NOP10	H/ACA ribonucleoprotein complex subunit 3
NPC	Nasopharyngeal carcinoma
NSCLC	Non-small cell lung cancer
PBLs	Peripheral blood leukocytes
PC	Prostate cancer
PCI	Phenol-chloroform-isoamylalcohol
PCR	Polymerase chain reaction
PIN	Prostatic intraepithelial neoplasia
PLB	Passive lysis buffer
PSA	Prostate specific antigen
R ²	coefficient of determination
RB	Retinoblastoma gene
RGS17	Regulator of G-protein signalling 17 gene
RHOB	Ras homology family member B
RNA	Ribonucleic acid
RPM	Revolutions per minute
SCLC	Small cell lung cancer
SDS	Sodium dodecyl sulfate
SNP	Single nucleotide polymorphism
SP1	Transcription factor SP1
SV40	Simian virus 40
TCAB1	Telomerase Cajal body protein 1
TERT	Telomerase reverse transcriptase gene/protein
TP53	Tumour protein p53
TR	Telomerase RNA component gene/protein
VNTR	Variable number of tandem repeat

1. Introduction

1.1. Prostate cancer

1.1.1. Epidemiology of prostate cancer

In 2012, an estimated number of 1.1 million men worldwide developed prostate cancer (PC). Hence, PC is the second most common cancer in men. Additionally, PC is the fifth common cause of cancer related death in men [4].

In Austria, PC is the most frequent cancer among male, with 69 incidences per 100.000 men, whereby old-age-groups have the highest incidence. The mortality is approximately 14 per 100.000 men (2011) [5].

From 1990 to 2003, a massive increase in PC incidence was detectable [3, 5], whereas mortality decreased minimal during this period [3]. Since 2003, the incidence rate exhibits a slow regression [3, 5]. Enhanced prostate-specific antigen (PSA) screening was accounting for the strong increase during the 1990s, whereas reduction after 2003 is referable to earlier detection of indolent, asymptomatic PC cases [3].

1.1.1. Molecular epidemiology of prostate cancer

Men in PC-affected-families [6-8] as well as with African origin [8, 9] have increased PC susceptibility, indicating a strong genetic influence on PC risk [8, 10].

Multiple genome wide association studies (GWAS) have detected 76 common single nucleotide polymorphisms (SNPs) associated with PC risk [11-31]. The 8q24 region, located near the MYC oncogene [11, 31] and involved in MYC expression regulation [32], contains multiple independent PC risk variants [11-14, 33, 34]. Adjacent to the MSMB (beta-microseminoprotein gene) transcription start site, chromosome 10 harbours rs10993994, associated with PC [16, 25, 35], which adversely affects the gene's expression level [36].

Since numerous PC susceptibility variants are located in noncoding regions, probably influencing enhancers, promoters or microRNA binding sites [37], the effects of only few

PC SNPs on prostate carcinogenesis has been resolved. The majority of identified risk variants have unresolved influence in prostate carcinogenesis, mainly serving only as PC risk markers [31].

Discrimination between indolent and aggressive PC cases is of special importance to avoid overtreatment of indolent cases, for which an observing strategy is beneficial. Hence, finding associations between susceptibility loci and PC aggressiveness is of central significance [10, 31, 38]. Some published studies advocate an association between some susceptibility variants and PC aggressiveness [39-41]. However, a meta-analysis postulated an association between only one risk variant at 17q12 and the aggressive disease form [42].

1.2. Lung cancer

1.2.1. Epidemiology of lung cancer

In 2012, 12.9% of all new cancer cases worldwide concern the lung. Hence, lung cancer is the most common cancer worldwide. Whereas lung cancer is the most frequent cancer among men in the world, in women the global number of new lung cancer cases is much smaller. Additionally, lung cancer is responsible for the most cancer related deaths in both sexes worldwide. The global number of lung cancer deaths in men is definitely higher than in women [4].

In Austria, sex differences, concerning lung cancer incidence and mortality, coincide with global gender variations [4, 43]. In Austria, lung cancer is the second most common cancer in men and the third most common cancer in women. It is the most frequent cancer related cause of death in men and the third most common in women [43].

Although the 1-year and 5-year relative survival rates for lung cancer have increased the last few decades [44], the current 5-year survival rate, including all tumour stages, is still very low [45]. Localized lung cancer has a 54.8% 5-year survival probability. The survival rate decreases to 27.4% for regional lung cancer and to only 4.2% for distant lung cancer disease [45]. However, majority of lung cancer cases are diagnosed at the later metastasized stage [44].

Although numerous diverse environmental risk factors (e.g. radon, nickel, beryllium, arsenic, cadmium, chromium, silica, asbestos [46] and HIV infection [47]) exist, cigarettes are the most important aetiological factors for developing lung cancer [48, 49]. Approximately 80-90% of new lung cancer cases arise from smoking [49, 50], whereas lung cancer emerges in 10-15% of cigarette smokers [49, 51].

1.2.2. Histology of lung cancer

Lung cancer has a high biological, clinical, histological and molecular heterogeneity [52]. Histological heterogeneity arises due to many different histological lung cancer types. Non-small cell lung cancer (NSCLC) and small cell lung cancer (SCLC) are the two major lung cancer types. They differ not only histologically and clinically but also molecularly, featuring various type-specific genetic modifications. Based on histological properties, NSCLC is additionally divided into adenocarcinoma, squamous carcinoma, large cell carcinoma, bronchoalveolar cancer and mixed histological types, also showing differences in molecular biology [52].

1.2.3. Molecular epidemiology of lung cancer

GWAS have revealed diverse SNPs in multiple genetic susceptibility loci for lung cancer (reviewed in [52, 53]). Although these variants are associated with lung cancer, the biological functionality related to lung cancer is not always clarified. Nevertheless, recognizing such polymorphisms as potential genetic risk factors and biomarkers may improve early diagnosis and lung cancer treatment [53].

A genome-wide linkage study identified 6p23-25 as susceptibility locus for familial lung cancer [54, 55]. Within this locus, variants of the possible causal RGS17 (member of the regulator of G-protein signalling family) gene were linked to familial lung cancer cases [56].

Additionally, several SNPs at the 15q24-25 chromosomal region, which harbours nicotine acetylcholine receptor (nAChR) subunits expressing genes, are linked to an increased risk of lung cancer [57-59]. The 6p21.33 locus, containing the BAT3 gene, represents a further lung cancer susceptibility locus [60-62]. Additionally, the 5p15.33 locus, containing the telomerase reverse transcriptase (TERT) gene [63], is an important susceptibility locus for lung cancer [60, 64, 65].

1.3. Telomeres and telomerase

1.3.1. Telomere structure and function

The natural ends of chromosomes consist of specialized functional DNA-Protein constructs, termed telomeres. In human cells, telomeric DNA is composed of the characteristic repetitive hexameric nucleotide sequence 5'- TTAGGG - 3' [66], resulting in approximately 10-kilobase pair long arrays [67, 68]. These arrays are associated with several copies of the shelterin protein complex, consisting of six subunits [66, 69].

The telomeres are involved in overcoming the chromosomal end-replication [70] and are additionally important in protecting the chromosomal ends [69].

Chromosomal ends, lacking telomeres and therefore shelterin complexes, can be mistaken as DNA damage site, leading to cell cycle arrest, chromosome end-to-end fusions and sequence exchange [71]. Hence, it is of prime importance for the cell to discriminate natural chromosomal ends from chromosomal broken ends and to protect the natural ends of linear DNA molecules from cellular DNA damage response pathways [69, 71]. Both, the telomeric structure plus the associated shelterin complexes are necessary for this end-protection, through telomere structure stabilization and by blocking the main DNA damage signalling and response pathways [71, 72].

Every DNA synthesis, proceeding in 5'-to-3' direction, requires initiation at the 3'-hydroxyl end of a DNA or of a RNA primer. For the lagging strand synthesis, RNA primer are positioned at the template DNA and are finally removed. This replication mechanism leads to the loss of certain number of bases at the lagging strand, resulting in a 3' single-strand overhang and successive telomere shortening [70]. Consequently, a gradual loss of telomeric base pairs in human cells occurs with increasing number of cell cycles or with increasing age [70, 73, 74]. Hence, telomeres become too short to shelter the natural ends of chromosomes. Consequently, replicative senescence and crisis occurs, associated with chromosomal end-to-end fusion, karyotypic instability, resulting in apoptotic cell death. This leads to a restricted proliferative capability of normal somatic cell lineages [75].

1.3.2. Telomerase and the hTERT gene

1.3.2.1. Telomerase structure and function

The telomerase enzyme is a highly regulated ribonucleoprotein complex containing a reverse transcriptase activity [76]. Telomerase adds telomeric hexanucleotids to extend telomeric DNA [77, 78], avoiding replicative senescence and crisis [75].

The core of the mammalian telomerase holoenzyme is composed of two subunits. The catalytic subunit is a protein with reverse transcriptase activity. The second part of the core subunit is a 451nt long telomerase-associated RNA molecule (TR or TER), which functions as RNA template for the catalytic subunit. In human cells, the two core subunits are denoted as hTERT (human telomerase reverse transcriptase) and hTR (human telomerase-associated RNA molecule) [75, 79].

Additionally, dyskerin (DKC1), a RNA-binding protein, is part of the telomerase holoenzyme. It stabilizes TR and participates in the biogenesis of the core complex [80]. Further, accessory subunits, such as NOP10 and NHP2, which are linked to DKC1, are involved in forming the telomerase holoenzyme [81, 82]. TCAB1, another subunit of the holoenzyme, guides the telomerase complex through the cajal bodies to the telomeres [83].

1.3.2.2. The hTERT gene

The hTERT gene is situated on chromosome 5p15.33 [63]. It consists of 15 introns and 16 exons [79]. Seven functional motifs, conserved among reverse transcriptases [1, 84], plus a telomerase-specific T motif [85, 86] are located in the hTERT gene. The promoter is made up of many CpG dinucleotides and multiple SP1 binding sites. The core promoter region encompasses 330bp upstream of the start codon ATG plus 37bp of exon 2. It does not possess either TATA or CAAT boxes. The promoter regulates the hTERT gene through an abundance of binding sites for a huge number of transcription factors, operating as activator or repressor [79, 85].

1.3.2.3. Telomerase activity regulation

High telomerase activity is detectable in germ cells, embryonic cells, self-renewing stem cell populations [76, 87] and in vitro immortalized cells [88]. Cell differentiation is associated with the decline of telomerase activity [89-91], resulting in inactive telomerase in most human somatic cells [75].

These differences of telomerase activity in distinct cell types [75, 76, 87, 88] point to a high enzymatic activity regulation. It seems to be controlled through transcriptional and post-translational regulation of hTERT and through transcriptional and post-transcriptional regulation of hTR. Additionally, enzyme modulation happens through telomerase recruitment to natural chromosomal ends [76].

Since the hTERT subunit is selectively expressed only in particular cell types [75, 76, 87, 88], whereas hTR expression is omnipresent [79], the control of the hTERT catalytic subunit and particularly the regulation of the hTERT gene promoter seems to be the major part in controlling telomerase activity [76, 79, 85]. In addition to transcriptional regulation of the hTERT promoter, the hTERT subunit is also modulated by post-translational phosphorylation and ubiquitination of hTERT. These post-translational modifications affect the hTERT stability, subcellular localization and further the telomerase activity [76].

1.3.3. Role of telomere and telomerase in tumorigenesis

1.3.3.1. Telomere shortening and carcinogenesis

As mentioned previously, the successive shortening of the telomeres results in replicative senescence in combination with cell growth arrest and activation of DNA damage pathways. Consequently, the replicative senescence, which normally retains cells in an inactive state for years, is a powerful tumour-suppressive mechanism to protect multicellular organisms against cancer development [82, 92].

Through genetic and epigenetic changes in cell cycle checkpoint genes (e.g. TP53 or RB), this inert state may be overcome, enhancing the proliferation of pre-cancerous cells. Due to this proceeded proliferation, chromosome end-to-end fusions occur, leading to dicentric chromosomes. Consequently, breakage-fusion-bridge events take place, followed by chromosomal translocations, aneuploidy and genomic instability. Finally, crisis, another powerful tumour-suppressive mechanism, associated with cell death, takes place. However, some cells may get out of crisis. Normally, almost all of these cells show telomerase activity, stabilizing the short telomeres and proceeding cell proliferation [82, 92]. Consequently, cancer cells proliferate infinitely, representing a hallmark of progressed human cancers [93, 94].

1.3.3.2. Telomerase activity in tumorigenesis

Telomerase activity, detectable in about 90% of human cancers [95], is important for an unlimited replicative potential, consequently playing a crucial role in tumorigenesis [92, 96].

Heaphy et al. [97] reports several studies, displaying different hTERT mRNA expression and diverse telomerase activity in malignant and benign tissues. Interestingly, telomerase activity was detected not only in malignant tissues but also in a few benign and pre-invasive lesions [98-100]. For instance, telomerase activity was measured in 84% of prostatic adenocarcinomas and also in 12% of neighbouring normal tissues but not in benign prostatic hyperplasia (BPH) tissues [98]. Additionally, Koeneman et al. [99] reported telomerase activity in 16% of high-grade prostatic intraepithelial neoplasia (PIN) tissues [99]. Further, expression analysis showed hTERT expression in most invasive prostatic cancers and in PIN lesions and moderate levels of hTERT expression in BPH lesions. However, in adjacent normal tissues almost no hTERT expression was detectable in this study [100]. Due to the finding that telomerase activity may be even present in benign and pre-invasive lesions, the usability of tissue telomerase activity as diagnostic biomarker seems to be limited [97].

1.3.3.3. Telomere length and cancer

Telomere length depends on the disease state and lifestyle [82, 101-105]. Additionally, it is influenced by telomere length inheritance, having various telomere lengths in different individuals at the time of birth [82, 106-108]. Consequently, this implicates individual-specific proliferative capability, leading to different numbers of possible cell divisions before telomere dysfunction proceeds. This may give rise to various cancer predispositions [82].

A link between the telomere length and the occurrence of cancer was detected. Shortening as well as lengthening are associated with increased cancer risk. These changes of telomere length often already occur in precursor lesions of human epithelial cancers. Furthermore, tissue telomere lengths are highly heterogeneous not only among distinct cancer types, but also within one cancer type and also within one tumour [97].

In PC for example, shortened tissue telomere lengths were observed, compared to BPH and to neighbouring normal tissue [99, 109]. Additionally, even in high-grade PIN abbreviated tissue telomeres were detected contrary to telomeres in normal prostatic epithelial cells

[110, 111]. However, telomere shortening was additionally monitored in histologically normal prostate tissues. Consequently, measuring the telomere lengths is probably not reasonable as a diagnostic marker of cancer [97].

Patients, suffering from NSCLC, also exhibit significantly shortened tissue telomere lengths in relation to normal tissue [112].

Additionally, different studies [113-115] have indicated associations between the peripheral blood leukocytes (PBLs) telomere length and enhanced cancer risk. Short PBL telomeres are significantly linked to a higher risk of lung, head, neck, bladder and renal cancer [113-115]. In contrast, there are no significant association between PBL telomere length and the risk of developing PC [116].

1.3.3.4. Association between hTERT locus genetic variants and cancer risk

The 5p15.33 region seems to play a critical role as susceptibility locus for many different cancer types. Many SNPs were identified within this locus, significantly associated with cancer risk, which are reviewed in Baird et al. [82]. Many associations between multiple individual 5p15.33 SNPs and a risk of developing diverse cancer types were described for lung cancer [60, 61, 64, 65, 117], basal cell carcinoma [65], glioma [118] and pancreatic [119], bladder, prostate and cervical cancer [65]. According to the cancer type, one SNP can be associated with an increased but also with a decreased risk for developing cancer [82]. rs401681, for example, is located adjacent to the hTERT gene and is significantly associated with an increased risk for lung, bladder, prostate and cervix cancer, and basal cell carcinoma [65] but also indicates a protective impact on melanoma genesis [65, 120].

The causal role of these SNPs is not utterly clarified, although the importance of telomere length and telomerase activity in tumour progression portend that SNPs within the hTERT locus play a critical role in tumorigenesis. The SNPs may have influence on the hTERT transcription and consequently on telomerase activity. SNPs within the hTERT control region may reverse transcriptional repression and thus result in increased proliferative potential [82].

Although 5p15.33 locus variants were identified as potential risk factors for cancer, findings from distinct studies do not always coincide. Consequently, these associations and the exact causative role of the different SNPs has to be further investigated [82].

1.4. MNS16A

Besides numerous existing SNPs within the 5p15.33 chromosomal band [60, 64, 65], the hTERT locus (Figure 1) harbours different variable noncoding mini- and microsatellites in introns, which distribute hTERT exons into four cluster. The fourth cluster contains additional mini- and microsatellites [1], whereas the second and third exon clusters host all seven known conserved reverse transcriptase motifs [1, 84].

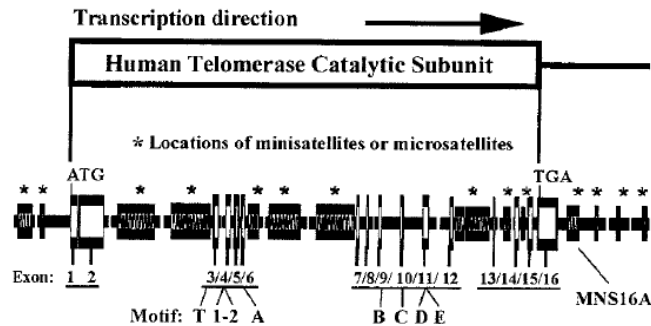


Figure 1. hTERT gene organisation. Indicating MNS16A position [1].

In a lung cancer study, Wang et al. (2003) [1] described an additional polymorphic tandem repeats minisatellite, termed MNS16A. It is located downstream of the hTERT exon 16 and upstream in the promoter region of an hTERT antisense transcript (Figure 2). This antisense transcript, containing two alternative starting points at nt 22156 and nt 22163 and only detectable in telomerase positive cells, might function as hTERT expression regulator [1].

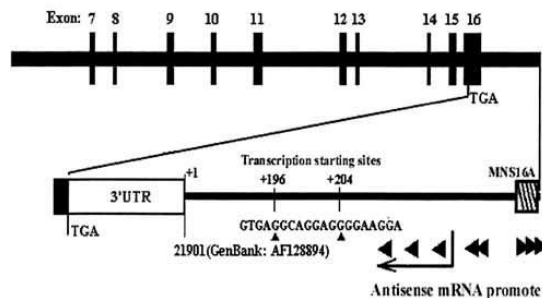


Figure 2. Promoter structure of hTERT antisense RNA [1].

MNS16A sequence includes two distinct repeat elements: a 23bp tandem repeat with TCC TCT TAT CTC CCA GTC TCA TC consensus sequence and a 26bp tandem repeat, containing a supplemental CAT trinucleotide insertion. The 26bp sequence with the CAT insertion represents a binding site for GATA-1 transcription factor [1].

Wang et al. (2003) [1] first detected four different MNS16A-VNTR alleles in several NSCLC cell lines, named (corresponding to PCR fragment size) VNTR-302, VNTR-243, VNTR-274 and VNTR-333. They differ in the number of the two distinct repeat elements. The wild-type VNTR-302 consists of two 23bp and three 26bp repeats, while VNTR-243 comprises of one 23bp and two 26bp repeat elements [1]. The rare VNTR-274 allele harbours one 23bp and three 26bp core sequences, whereas the rare VNTR-333 consists of two 23bp and four 26bp repeat elements [1, 2]. For statistical analysis, the four proved MNS16A variants were ranged in short (S) alleles (243 and 272) and long (L) alleles (302 and 333), getting three different genotypes: LL, SS and SL [1]. Hofer et al. (2011) [2] detected an additional MNS16A variant, named VNTR-364 (L allele), in a colorectal cancer study. VNTR-364 is similar to VNTR-333, however harbouring an extra tandem repeat element, containing an additional CAT insertion. Overall, five different allele variants were detected in this study, resulting in ten distinct genotype patterns [2]. Furthermore, Hofer et al. (2013) [3] described a sixth rare MNS16A variant, named VNTR-212 (S allele), in a PC study, resulting in eleven detectable genotype patterns. Representing the smallest allele variant, it is one tandem repeat shorter than VNTR-243, consequently harbouring the smallest quantity of binding sites for GATA-1 [3]. The core tandem repeat sequences of the different MNS16A alleles are shown in the appendix.

Due to detection of GATA-1 binding sites within MNS16A, Wang et al. (2003) [1] even investigated potential functionality of this minisatellite. Luciferase assay was conducted to examine the promoter activity of the VNTR-302 and VNTR-243 MNS16A. Lung cancer cell line H1299 was transfected with the pGL3-660 (S) plasmid construct, including a hTERT downstream 660pb fragment (contains the longer allele), and the pGL3-570 (S) construct, covering a hTERT downstream 570bp fragment (includes the shorter allele). H1299 cells, transfected with pGL3-660, show less strongly luciferase activity compared to cells, transfected with pGL3-570, suggesting MNS16A promoter activity and dependence of promoter activity on the number of MNS16A tandem repeats. The association between promoter activity and the length of the VNTR sequence were confirmed, using plasmid constructs (pGL3-243 and PFL3-302) only covering MNS16A core tandem repeats. According to these findings, it was hypothesized that MNS16A participates in expression regulation of the hTERT antisense RNA. MNS16A might function as potential repressor for antisense RNA promoter, affecting the repression of the hTERT expression [1].

2. Aim of the study

MNS16A is a polymorphic tandem repeats minisatellite in the promoter region of the antisense transcript of hTERT. Aim of this thesis was to investigate the potential promoter activity of the six currently known MNS16A VNTRs using a Dual-Luciferase reporter assay system in various lung and prostate cancer cell lines.

Further, the present thesis aimed to assess, whether MNS16A promoter activity is correlated with VNTR length. In addition, it was investigated if functionality differs in the used cancer cell lines.

3. Materials and methods

3.1. Molecular biology

3.1.1. Cloning

Table 1 lists all plasmid vectors. The vector maps can be found in the appendix. Sequence analysis for cloning was carried out, using Clone Manager Professional software version 9.0.

Plasmid vector	Obtained from	Product Number
pCRII-TOPO	Thermo Fisher Scientific; USA, Massachusetts	K4610-20
pGL3 CMV	Dr. Hedwig Sutterlüty-Fall laboratory	-
pRL-SV40 Renilla Luciferase Control Reporter Vector	Promega; USA, Wisconsin	E2231
pGL3 basic Firefly Luciferase Reporter Vector (Promoterless)	Promega; USA, Wisconsin	E1751
pAdlox CFP	Dr. Hedwig Sutterlüty-Fall laboratory	-

Table 1. All used plasmid vectors are listed.

3.1.1.1. Restriction digests

MNS16A VNTRs were cloned out of pCRII-TOPO and ligated with pGL3-basic vector, using restriction enzymes, listed in table 2 and table 3.

MNS16A	1.Restriction enzyme	1. Buffer	2. Restriction enzyme	2. Buffer	
VNTR-364	Xho I	H	Hind III	H	Double digestion
VNTR-333	Xho I	H	Sac I	A	Single digestion
VNTR-302	Xho I	H	Sac I	A	Single digestion
VNTR-274	Xho I	H	Sac I	A	Single digestion
VNTR-243	Xho I	H	Sac I	A	Single digestion
VNTR-212	EcoR V	B	Sac I	A	Single digestion

Table 2. All used restriction digestions are listed.

Vector DNA	1.Restriction enzyme	1. Buffer	2. Restriction enzyme	2. buffer	
pGL3-basic	Xho I	H	Hind III	H	Double digestion
pGL3-basic	Xho I	H	Sac I	A	Single digestion
pGL3-basic	SmaI	A	Sac I	A	Double digestion

Table 3. All used restriction digestions are listed.

15µl DNA, mixed with 5µl of the appropriate 10xbuffer, with 0.6µl from each restriction enzyme and with 2µl Bovine Serum Albumin (BSA), was filled up with ddH₂O to a final volume of 50µl. The approach was incubated for at least one hour at the appropriate cleavage temperature at the thermo block.

As an exception, 4µl pGL3-basic DNA, necessary for ligation with VNTR-212, was

digested in a final volume of 20µl, using 0.6µl from each enzyme, 2µl BSA and 2µl 10xbuffer.

Single digests were accomplished for most of the plasmid vectors, cutting DNA in two sequentially performed single digests. The purification step in between was performed by miniQuick Spin DNA Columns (product no. 11814419001), received from Roche Applied Science (Germany, Penzberg).

Sephadex G-50 matrix, prepared with 1xSTE buffer (10mM Tris/HCl pH 8, 1mM EDTA, 100mM NaCl), was used as described in the manufacturer's protocol. Flipping the column repeatedly, the matrix was resuspended. The column, placed in a 1.5ml tube, was centrifuged two times at 1000g for 1 minute with Eppendorf Centrifuge 5415C (Germany, Hamburg), before it was placed in a fresh tube and the digestion approach was put onto the matrix. Eluting DNA, the column was centrifuged at 1000g for 4 minutes.

The second single digest was performed, mixing the eluate with 5µl 10xbuffer, with 0.6µl of the second enzyme and with 2µl BSA, before incubation.

The used buffers obtain the following components:

Buffer A:

33mM TrisAcetat
10mM Magnesium-Acetate
66mM Potassium-Acetate
0.5mM Dithiothreitol (DTT)
pH at +37°C 7.9

Buffer M:

10mM Tris/HCl
10mM magnesium chloride
50mM sodium chloride
1mM Dithioerythritol (DTE)
pH at +37°C 7.5

Buffer H:

50mM Tris/HCl
10mM magnesium chloride
10mM sodium chloride
1mM Dithioerythritol (DTE)
pH at +37°C 7.5

Buffer B:

10mM Tris/HCl
5mM magnesium chloride
100mM sodium chloride
1mM 2-mercaptoethanol
pH at +37°C

Buffer L:

10mM Tris/HCl
10mM magnesium chloride
1mM Dithioerythritol (DTE)
pH at +37°C 7.5

Restriction enzyme	Recognition sequence	Cleavage temperature	Buffer activity
BamH I <i>Bacillus amyloliquefaciens</i>	G↓G°AT°C°C	+37° Celsius	B (100%)
EcoR V <i>Escherichia coli</i>	G°AT↓AT°C	+37° Celsius	B (100%)
Hind III <i>Haemophilus influenzae</i>	*A↓°AG°CTT	+37° Celsius	B (100%) A u. H (50-75%)
KpnI <i>Klebsiella pneumoniae</i>	GGTAC↓C	+37° Celsius	L (100%) A (75-100%)
Mlu I <i>Micrococcus luteus</i>	°A↓°CGCGT	+37° Celsius	H (100%)
Sac I <i>Streptomyces achromogenes</i>	G°AG°CT↓C	+37° Celsius	A u. L (100%) M (50-75%)
SFi 1 <i>Streptomyces fimbriatus</i>	GG°C°CNNNN↓NGG°C°C	+50° Celsius	M (100%) L (75-100%)
Sma I <i>Serratia marcescens</i>	*C°C°C↓GGG	+25° Celsius	A (100%)
Xba I <i>Xanthomonas campestris</i>	T↓°CTAGA	+37° Celsius	A u. H (100%) B, L u. M (75-100%)
Xho I <i>Xanthomonas campestris</i>	*C↓T°CG°AG	+37° Celsius	H (100%) B (75-100%)

Table 4. All used restriction enzymes are listed.

Bovine Serum Albumin (BSA):

20mg/ml in

50mM Tris/HCl

0.1M NaCl

0.25mM EDTA

1mM 2-mercaptoethanol

50%(v/v) glycerol

pH approximately 7.6

All used buffers, enzymes and the Bovine Serum Albumin (BSA) were obtained from Roche Applied Science.

3.1.1.2. Agarosegelelektrophorese

1.2% agarose gel was used after restriction digestion of pCRII-TOPO vectors, whereas digestions of pGL3-basic vector were loaded onto 0.8% agarose gel.

PeqGold Universal Agarose (PEQLAB Biotechnologie GmbH; Germany, Erlangen) was dissolved in 100ml 1xTAE buffer by heating the mixture. 1xTAE buffer served as running buffer. The whole digestion approaches were mixed with 6x loading buffer. 5µl λ marker (marker photo see Appendix) were used for each gel. 50 Volt were applied to the gel constantly using Electrophoresis Power Supply-EPS 200 (Pharmacia Biotechnology; Sweden, Stockholm) until the samples leaved the slots. Afterwards voltage was increased to 100 Volt. The gel was incubated in a 0.25µg/mL ethidium bromide solution for about 20 minutes and viewed under ultraviolet light using GelDoc detection system (Bio-Rad Laboratories; USA, California).

	Dissolved in ddH ₂ O, pH 8.3
Components	Acquired from
0.04M Tris acetate	-
1mM EDTA	GERBU Biotechnik GmbH (Germany, Heidelberg)

Table 5. Components of 1xTAE

	Diluted in 1xTE
Components	Acquired from
40% saccharose	MERCK KGaA (Germany, Darmstadt)
24% urea	MERCK KGaA
0.25% xylene blue	MERCK KGaA
0.25% bromphenol blue	MERCK KGaA

Table 6. Components of 6xloading buffer

0.25µg/ml ethidium bromide solution:

Ethidiumbromid (1µl/ml), obtained from AppliChem (Germany, Darmstadt) was diluted in 1xTAE.

λ Marker:

λ-DNA (0.3µg/µl), purchased from Fermentas International Incorporation (Canada, Ontario) was digested by HindIII and EcoRI.

	Incubate at 37°C overnight
Components	Acquired from
200µl λ-DNA	FermentasInternational Incorporation
42µl Hind III	Roche Applied Science
42µl EcoRI	Roche Applied Science
167µl ddH ₂ O	-

Table 7. Production of λ marker

3.1.1.3. DNA fragment extraction from gel

QIAquick Gel Extraction Kit (cat. Nos. 28704 and 28706) from Qiagen (Netherlands, Limburg; Germany, Hilden) was used to extract correct DNA fragments out of agarose gel under UV light.

According to manufacturer's protocol, 3 volumes QG buffer were added to 1 volume gel (100mg gel ~ 100µl). It was incubated at 50°C for 10 minutes at 900rpm. 10µl 3M sodium acetate (MERCK KGaA) pH 5.0 were added, if color of the solution was not yellow.

After adding 1 volume isopropanol (MERCK KGaA), sample mixing and very short centrifugation with Eppendorf Centrifuge 5415C, the sample was applied to the QIAquick column. Centrifugation at 13.000rpm for 1 minute at room temperature was done with Eppendorf Centrifuge 5417R (Germany, Hamburg) repeatedly until the whole sample passed the column. 500µl QG buffer were added, followed by centrifugation. Removing the flow-through, 750µl PE Buffer were added. After 3-5 minutes incubation, the sample was centrifuged repeatedly.

The spin column was placed in a new tube, eluting pGL3-basic vector DNA with 50µl and MNS16A insert DNA with 30µl ddH₂O.

3.1.1.4. Ligation

Using Rapid DNA Ligation Kit (product no. 11635379001) from Roche Applied Science, 4µl VNTR-364 insert was ligated with 2µl pGL3-basic vector, digested with Hind III and with Xho I, while 5µl VNTR-212 was ligated with 2µl pGL3-basic vector, digested with Sma I and with Sac I. For the remaining VNTRs, 5µl were ligated with 2µl pGL3-basic vector, digested with Xho I and Sac I.

For each pGL3 digestion variant a vector control was performed during ligation.

1% agarose gel was carried out, estimating molar concentration of eluted insert and vector DNA. 5µl DNA, mixed with 1µl 6xLoading buffer were loaded, performing electrophoresis.

Insert DNA, vector DNA, 5x DNA Dilution buffer and 2x T4 DNA Ligation buffer were gently mixed. Appropriate amounts of insert and vector DNA were mixed with the respective volume of ddH₂O to get a final volume of 8µl. 2µl 5x DNA Dilution buffer were added to receive a final volume of 10µl. After merging, 10µl 2x T4 DNA Ligation buffer and 1µl T4 DNA Ligase were added and the approach was mixed gently by pipetting up and down. Following incubation for 20 minutes at room temperature, competent E.Coli XL-1 bacteria cells, received from Dr. Hedwig Sutterlüty-Fall laboratory, were transformed with the whole ligation approach.

3.1.1.5. E. Coli transformation

Competent E.Coli XL-1 bacteria and plasmid DNA were defrozen on ice. 100µl of competent XL-1 bacteria were added to 1µl DNA. After incubation on ice for 20 minutes, the bacteria were put into water bath for 90 seconds at 42°C and finally incubated on ice for 2 minutes.

Bacteria were plated on selective LB agar dishes (SARSTEDT AG u. Co.; Germany, Nürnberg), containing Ampicillin (AppliChemGmbH). Bacterial culture dishes were incubated at 37° C overnight in the Heraeus® Function Line incubator (Heraeus Holding GmbH; Germany, Hanau).

For transforming bacteria cells with the ligation approaches, 200µl LB medium were added and the bacteria were shaken at 37°C for 20 minutes at 300rpm, before plating on ampicillin selective agar plates (Amp⁺).

Ampicillin (100mg/ml) was dissolved in ddH₂O, filtered sterile through a 0.45µm nitrocellulose filter (NalGene, Thermo Scientific; USA, Massachusetts) and stored at -20° C.

For selective LB Agar plates (Luria-Bertani Agar), 14g (35g/l) LB-Agar, obtained from Sigma-Aldrich (USA, Missouri) were filled up to 400ml. LB-Agar were autoclaved and after cooling down, 400µl Ampicillin were added. The LB-Agar was poured into dishes and after curing, the plates were put into the fridge.

3.1.1.6. STETL (Sucrose-Triton-EDTA-HCl-Lysozyme) mini-preparation

Vector preparation from positive clones was carried out by STETL Mini Preparation, starting with inoculation in 3ml LB-Medium overnight at 180rpm and 37°C in the GFL 3031 shaking incubator (Gesellschaft für Labortechnik mbH; Germany, Burgwedel).

Cultures were centrifuged at 10.000g for 3 minutes with Eppendorf Centrifuge 5417R. Pellets, resuspended in 110µl STETL buffer, were incubated for 1 minute at 95°C and centrifuged at 10.000g for 10 minutes at 4°C. Using an autoclaved toothpick, which was first dipped in RNaseA, the pellets were removed. 110µl isopropanol (MERCK KGaA) was added and mixed. The solution was centrifuged at 10.000g for 15 minutes at 4°C. Pellets were washed twice with 200µl ice cold 70% ethanol (MERCK KGaA). Following a 15 minutes drying period at room temperature, plasmid vectors were dissolved in 30µl ddH₂O and stored at -20°C.

5µl DNA from each STETL preparation, mixed with 10xbuffer, 0.3µl enzymes and 1µl BSA, were filled up with ddH₂O to 25µl, performing restriction digestion as already described. The whole amount of restriction approaches, mixed with 6xloading buffer, was put onto a 1.2% agarose gel, controlling success of the ligations.

STETL Buffer diluted in ddH₂O

Components	Acquired from
8% Sucrose	United States Biochemical CORP. (USA, Ohio)
0.5% Triton X-100	-
50mM Tris/HCl pH8	MERCK KGaA
50mM EDTA pH8	GERBU Biotechnik GmbH
0.05% Lysozyme, added freshly	Roche Applied Science

Table 8. Components of STETL buffer

Components	Acquired from
10mM Tris/HCl pH 7.5	MERCK KGaA
15mM NaCl	MERCK KGaA
5% Ribonuclease A	Sigma-Aldrich

Table 9. Components of RNaseA

8g (10g/l) LB-Broth, obtained from Sigma-Aldrich, were filled up to 400ml with ddH₂O before autoclaving. 400µl Ampicillin were added before use.

Components

10g/l Tryptone (pancreatic digest of casein)

5g/l Yeast extract

5g/l Natriumchlorid

Table 10. Components of LB medium

3.1.2. DNA purification by cesium chloride banding

Cloned MNS16A VNTRs as well as pGL3-basic, pGL3 CMV, pRL-SV40 and pAdlox CFP vector DNA were purified, using cesium chloride density gradient centrifugation.

Following transformation of competent E. Coli XL-1 bacterial cells with different plasmid DNA and overnight incubation on amp⁺ selective agar plates, one colony was picked and inoculated in 3ml amp⁺ LB Medium at 180rpm and 37°C in the GFL 3031 shaking incubator. 8-9 hours later, cultures were put into 500ml LB Medium (amp⁺), incubating at 180rpm overnight at 37°C.

Cultures were centrifuged at 5000rpm for 5 minutes at room temperature, using SORVALL RC6 centrifuge (Thermo Electron Corporation; USA, Massachusetts) and PTI F14S-6x250y rotor (Thermo Electron Corporation; USA, Massachusetts). Pellets were resuspended in 15ml LB medium, containing ampicillin, and transferred into SS34 centrifugation tubes. Centrifugation at 10.000rpm for 10 minutes at room temperature was performed. FIBERLite F21-8x50y from Thermo Electron Corporation was utilized as rotor. Pellets were retained at -20°C.

Thawing bacterial pellets on ice, they were dissolved in 1ml 25% Sucrose. Following 30 minutes incubation on ice, 200µl 1% lysozyme solution (Roche Applied Science) was added. After mixing and incubating 10 minutes on ice, 400µl 0.25 EDTA pH 8 (GERBU Biotechnik GmbH) were added. Following 10 minutes incubation on ice, 1.6ml Triton X-100 (lytic mix) were added, mixed and incubated 20 minutes on ice. Lysed bacteria cells were centrifuged at 16.000rpm for 30 minutes at 4°C with SORVALL RC6 Centrifuge and FIBERLite F21-8x50y rotor.

Supernatant was filled up with TES buffer to 5.5ml and 0.97g cesium chloride (AppliChem GmbH) per 1ml liquid was added. Quick-Seal tubes (Beckmann Coulter Inc.; USA, California) were filled up with 100µl ethidiumbromide (AppliChem GmbH) and DNA solution. The tubes were welded with a metal cap, avoiding air bubbles. For ultracentrifugation at 55.000rpm for 22 hours at 14°C, Optima L-100 XXP centrifuge and NVTI 65-2 rotor from Beckmann Coulter Inc. were used.

After centrifugation, two distinct bands were visible. The lower band was drawn off, using an 18G needle (HENKE SASS WOLF GmbH; Germany, Tuttlingen) and a BD Discardit II 2ml syringe (Becton Dickinson and Company; USA, New Jersey).

A second round ultracentrifugation at 55.000rpm for at least 18 hours at 14°C was performed, using 1g cesium chloride per 1ml liquid and 75µl ethidium bromide per tube. The lower band was drawn off.

DNA solution, filled up with T/E pH 8 to 6ml, was mixed with 2.5 volumes 100% (room temperature) ethanol (MERCK KGaA) in SS34 tubes. After incubation at -80°C for at least 1 hour, centrifugation at 13.000rpm for 15 minutes at 4°C was performed. DNA pellets were dried and dissolved in 1ml 0.5% SDS (Sigma-Aldrich).

Two Phenol – Chloroform- Isoamylalcohol (PCI) extractions were performed, using 500µl PCI (Sigma-Aldrich). After centrifugation at 10.000rpm for 10 minutes with Heraeus PIC017 centrifuge from Thermo Electron Corporation, aqueous phases were taken off.

DNA was filled up to 6ml with T/E pH 8. 2.5 volumes 100% ice cold ethanol (MERCK KGaA) and 600µl 3M sodium acetate(MERCK KGaA) pH 5.3 were added and incubated at -20°C for at least 1 hour. After centrifugation and dissolving DNA pellets in 1ml 0.5% SDS, one PCI extraction and one Chloroform -Isoamylalcohol(1:24) extraction (AppliChem GmbH–MERCK KGaA) were done, followed by an ethanol precipitation at -20°C overnight.

DNA were pelleted and resuspended in 500µl T/E pH 7. Concentrations were measured by NanoDrop ND-1000 spectrophotometer (PEQLAB Biotechnologie GmbH; Germany, Erlangen) at 260nm, using 1µl T/E pH 7 as blank.

After a further overnight ethanol precipitation, DNA pellets were resuspended in an adequate amount of T/E pH7, reaching a final concentration between 400ng/µl and 500ng/µl.

Using between 250 and 500ng DNA, mixed with 10xbuffer, 0.3µl from each enzyme and 1µl BSA and filled up to 15µl with ddH₂O, control digestion was performed.

Some Preparations of MNS16A VNTRs were digested, using Kpn I, Hind III and buffer A. pGL3-basic, pRL-SV40 and pGL3 CMV DNA were digested, shown in table 11.

DNA vector	1.Restriction enzyme	2. Restriction enzyme	Buffer	
pGL3-basic	Hind III	BamH I	B	Double digestion
pGL3 CMV	Mlu I	Xba I	H	Double digestion
pRL-SV40	Hind III	BamH I	B	Double digestion
pAdlox CFP	Sfi 1	-	A	Single digestion

Table 11. Restriction digestions after cesium chloride banding.

Additionally to restriction digestions, 1µl plasmid DNA, diluted in 9µl T/E pH 7 and mixed with 2µl 6xloading buffer, was loaded on 0.8-1.2% agarose gels.

For DNA preparations, still carrying ethidium bromide, further overnight ethanol precipitations were carried out.

TES-Buffer	Filled up with ddH ₂ O
Components	Acquired from
1M Tris/HCl pH8	MERCK KGaA
0.25M EDTA pH8	MERCK KGaA
5M sodium chloride	MERCK KGaA
Sucrose-Solution	Filled up with ddH ₂ O
Components	Acquired from
25% Sucrose	United States Biochemical CORP.
1M Tris/HCl pH8	MERCK KGaA
0.25M EDTA pH8	MERCK KGaA
Triton X-100 Lytic Mix	Filled up with ddH ₂ O
Components	Acquired from
0.25M EDTA pH8	MERCK KGaA
1M Tris/HCl pH8	MERCK KGaA
10% Triton	Sigma-Aldrich
T/E pH 8 (7)	Filled up with ddH ₂ O
Components	Acquired from
10mM Tris/HCl pH 8 (7)	MERCK KGaA
1mM EDTA pH 8 (7)	MERCK KGaA

Table 12. Production of different solutions used for cesium chloride banding

3.2. Cell biology

3.2.1. Cell lines

All used human lung and prostate cancer cell lines are listed in table 13. They were established either from the American Type Culture Collection (ATCC) company or from the Institute of Cancer Research (ICR), Medical University of Vienna.

Cell line	Derived from	Tissue	Cell type	Disease
A-427	ATCC	Lung	Epithelial cell	Adenocarcinoma
A-549	ATCC	Lung	Epithelial cell	Adenocarcinoma
Calu-6	ATCC	Unknown; probably lung	Epithelial cell	Anaplastic carcinoma
SK-LU-1	ATCC	Lung	Epithelial cell	Adenocarcinoma
Calu-3	ATCC	Lung; metastatic site, pleural effusion	Epithelial cell	Adenocarcinoma
HCC827	ATCC	Lung	Epithelial cell	Adenocarcinoma
NCI-H1650	ATCC	Lung; metastatic site, pleural effusion	Epithelial cell	stage 3B, bronchoalveolar carcinoma
LXF-289	DSMZ	Lung	Epithelial cell	Adenocarcinoma
SW1573	ATCC	Lung	Epithelial cell	Alveolar cell carcinoma
VL-8	ICR	Lung; metastatic site, lymph node	Epithelial cell	Squamous cell carcinoma
VL-7	ICR	Lung; metastatic site, lymph node	Epithelial cell	Squamous cell carcinoma
VL-3	ICR	Lung	Epithelial cell	Squamous cell
VL-5	ICR	Lung; metastatic site, lymph node	Epithelial cell	Squamous cell
VL-2	ICR	Lung	Epithelial cell	Large cell carcinoma
VL-4	ICR	Lung	Epithelial cell	large cell carcinoma
PC-3	ATCC	Prostate; metastatic site, bone	Epithelial cell	Adenocarcinoma, grade IV
LNCaP	ATCC	Prostate; metastatic site, lymph node	Epithelial cell	Carcinoma
DU 145	ATCC	Prostate; metastatic side, brain	Epithelial cell	Carcinoma

Table 13. All used cancer cell lines.

3.2.2. Cell cultivation

All working steps were performed under sterile conditions in the HOLTEN LAMINAIR laminar. Heracell™ 150 incubator from Thermo Electron Corporation was used for cell line incubation and CK40 inverted phase contrast microscope from Olympus Corporation (Japan, Tokyo) was used for everyday work in cell culture laboratory.

Except for VL-7, cultured in 10ml RPMI-1640 medium (Sigma-Aldrich), all cell lines were cultured in 10ml (DMEM) Dulbecco's modified eagle's medium (Sigma-Aldrich) with 10% (FCS) fetal calf serum (Gibco®; Life Technologies; USA, California) and with Penicillin and Streptomycin. The cell lines, if not mentioned otherwise, were incubated at

37°C with 7.5% CO₂ on 100x20mm culture dishes (Becton, Dickinson and Company; USA, New Jersey).

For passaging, cells were washed with 5ml 1xPBS and trypsinized with 1ml Trypsin/EDTA.

Frozen cells were thawed at 37° C and transferred in about 10ml DMEM medium for centrifugation at 800rpm for 5 minutes by Heraeus Megafuge 1.0R (Heraeus Holding GmbH; Germany, Hanau). Cells were resuspended in 10ml DMEM medium and transferred onto a culture dish. Medium was changed the next day.

For long-time storage, trypsinized and resuspended cells were centrifuged at 800rpm for 5 minutes. The pellet was resuspended in 1ml freezing medium (10% (DMSO) Dimethylsulfoxid (AppliChem GmbH) with heat inactivated FCS) and transferred into cryopreservation tubes (NALGENE Cryoware from Thermo Scientific). The tubes were put on ice immediately. For long-time storage, the frozen cells were stored in liquid nitrogen after 24 hours at -20° C.

10xPBS	
Components	Acquired from
137mM NaCl	MERCK KGaA
2.7mM KCl	MERCK KGaA
4.3mM Na ₂ HPO ₄ ·2H ₂ O	MERCK KGaA
1.4mM KH ₂ PO ₄	MERCK KGaA

Trypsin	
Components	Acquired from
0.1% Trypsin	-
0.01% EDTA	-
0.001% phenolred	-

Table 14. Production of different solutions used for cell cultivation.

3.2.3. Calcium phosphate transfection

DNA, used for transient calcium phosphate transfection, was prepared by cesium chloride density gradient centrifugation.

3.2.3.1. CFP-DNA transfection

Cell lines, listed in table 3.16, were transfected with pAdlox CFP vector, containing cyan fluorescent protein, using transient calcium phosphate transfection method.

Between 100.000 and 200.000 cells, depending on the growth rate of the different cell lines, were seeded to 60x15mm culture dishes (Becton, Dickinson and Company) and incubated

24 hours before transfection. Bürker-Türk cell counter was used to determine the cell number of the particular single cell suspensions.

Per cell line eight different approaches, listed in table 15, were performed simultaneously.

Buffer	Calcium chloride	Transfected DNA	End volume DNA CaCl ₂ mixture	Glycerol shock
240µl 2xHBS	30µl 2M CaCl ₂	10µg	240µl	No
240µl 2xHBS	30µl 2M CaCl ₂	10µg	240µl	Yes
120µl 2xHBS	15µl 2M CaCl ₂	5µg	120µl	No
120µl 2xHBS	15µl 2M CaCl ₂	5µg	120µl	Yes
250µl BBS	25µl 2.5M CaCl ₂	10µg	250µl	No
250µl BBS	25µl 2.5M CaCl ₂	10µg	250µl	Yes
125µl BBS	12,5µl 2.5M CaCl ₂	5µg	125µl	No
125µl BBS	12,5µl 2.5M CaCl ₂	5µg	125µl	Yes

Table 15. Eight different transfection approaches were used for each cell line.

All used reagents and pAdlox CFP DNA were kept at 25°C before transfection.

DNA was mixed, in the following order, with ddH₂O and CaCl₂ to reach the appropriate end volume of the DNA CaCl₂ approach. The mixture was mixed by pipetting up and down, before it was transferred to the same volume of the particular buffer, while generating air bubbles in the buffer continuously. Following incubation at room temperature for exactly 20 minutes, DNA mixture was added dropwise to the cells, after the conditioned medium was removed. Incubating the cells exactly 5 minutes at room temperature, the primarily removed medium was added to the cells and the cells were incubated overnight. Cells, transfected with BBS buffer, were incubated at 3% CO₂ until medium was changed.

Four out of eight approaches were used to perform glycerol shock three to five hours later, adding 1.5ml 15% glycerol (GERBU Biotechnik GmbH) solution, diluted in 1xHBS, to medium free cells. After incubation for 30 seconds to 1 minute at 37°C with 7.5% CO₂, glycerol solution was removed. Cells were washed twice with 3ml 1xPBS and incubated overnight with finally 5ml medium.

Incubation of the cells was continued until day 3 after transfection, with two wash steps in between, on day one and two after transfection. For sensitive cell lines additional wash steps were performed on day one after transfection.

3.2.3.2. MNS16A VNTRs transfection

Performing luciferase assay, 200.000/300.000 A-427 and 175.000 LNCaP cells were used for transient calcium phosphate transfection method. Nine transfection approaches were accomplished simultaneously.

For six approaches, co-transfection with 10µg of one of the six MNS16A VNTRs plus 3µg

pRL-SV40 Renilla was performed while the other approaches were co- transfected with pGL3 basic/pRL-SV40 and with pGL3 CMV/pRL-SV40 DNA. 13µg DNA were mixed with ddH₂O and with 39µl 2M calcium chloride to reach an end volume of 312µl. 312µl 2xHBS were used for each transfection. One untransfected approach was used as blank during luciferase assay. No glycerol shock was performed.

Instead of 3µg pRL-SV40 DNA 5µg were used for the first three transfections of LNCaP.

For the rest, transfection method was performed accordingly to the protocol described for pAdlox CFP transfection.

HEPES Bufferes Saline	
Components	Acquired from
250mM NaCl	MERCK KGaA
10mM KCl	MERCK KGaA
12mM dextrose	Sigma-Aldrich
50mM 2-(4-(2-Hydroxyethyl)-1-piperazinyl)-ethansulfonsäure (HEPES)	Sigma-Aldrich
1.5mM Na ₂ HPO ₄ x2H ₂ O	MERCK KGaA
BES-buffered solution (BBS)	
Components	Acquired from
50mM N,N-bis(2-hydroxyethyl)-2-aminoethanesulfonic acid (BES)	
280mM NaCl	MERCK KGaA
1.5mM Na ₂ HPO ₄ x2H ₂ O	MERCK KGaA

Table 16. Production of two different buffers for CFP transfection.

pH value of 2xHBS buffer was adjusted exactly at 7.05 using 0.5M NaOH (MERCK KGaA) whereas the pH value of BBS buffer was adjusted exactly at 6.95 with 1M NaOH after dissolving the reagents in ddH₂O. The buffers were sterilized with a 0.45µm nitrocellulose filter and stored at -20° C.

2M or 2.5M CaCl₂ (MERCK KGaA) was dissolved in ddH₂O, sterilized with a 0.45µm nitrocellulose filter and stored at -20°C.

3.2.4. Determination of transfection efficiency

Eclipse TE300 inverted microscope (Nikon; Tokyo, Japan) was used to investigate cells, transfected with pAdloxCFP DNA. Exposure time was adjusted to 5000ms for fluorescence and to 0,5ms for phase contrast imaging.

Fluorescence illumination was performed, using X-Cite Series 120PC fluorescent lamp (Olympus Corporation; Tokyo, Japan).

MetaMorph® Microscopy Automation & Image Analysis Software (Molecular Devices; USA, California) and the 18.0 Monochrome W/O IR camera (Nikon; Japan, Tokyo) were utilized to take phase contrast as well as fluorescence images.

3.2.5. Dual-Luciferase reporter assay

Measuring MNS16A promoter activities from A-427 and LNCaP cell lines, Dual-Luciferase® Reporter (DLR™) Assay System (E1910) from Promega was used, following the manufacture's protocol. It depends on co-transfection of two different luciferases, Firefly and Renilla, whereby Firefly luciferase (pGL3 vector) was used as experimental and Renilla luciferase (pRL-SV40 vector) served as internal control reporter.

Preparing cell lysate, active lysis of cells was performed by scraping. After two wash steps with 3ml unsterile 1xPBS, 400µl 1xPLB (Passive Lysis Buffer) were added to the cells, immediately harvested by scrapping. Lysate was transferred into a tube and pipetted several times up and down. Two freeze–thaw cycles were carried out, using liquid nitrogen and water bath at 37°C. Cell lysate was cleared from cell debris by centrifugation 30 seconds, using Heraeus PICO 17 Centrifuge. The cell lysate was kept at room temperature.

Activity of Firefly luciferase was measured, adding 100µl LARII to 20µl lysate, using white Opaque OptiPlate™-96 Microplates (PerkinElmer; USA, Massachusetts). LARII and the lysate were mixed by pipetting two times up and down. Measuring luciferase activity, by a 10-second measurement period for each reaction, Synergy HT Multi-Mode Microplate Reader (BioTek U.S.; USA, Vermont) was used. After Firefly measurement, 100µl Stop and Glo® Reagent were added to the lysate-reagent mixture, quantifying Renilla Luciferase. Mixing and measurement Renilla Luciferase were done as before.

Both, Firefly and Renilla Luciferase activities were measured at the following instrumental settings, listed in table 3.21.

Detection Method	Luminescence
Read Type	Endpoint
Integration Time	10.0 SS.s
Emission	Hole
Optics Position	Top
Sensitivity	135
Top Probe Vertical Offset	1.00mm

Table 17. Instrumental setting for measuring luciferase activities.

The lysate of untransfected cells plus luciferase reagents served as blank. Promoterless pGL3-basic vector worked as negative and Firefly luciferase CMV-vector as positive control. To use a cell line for luciferase assay, Firefly activity of positive control had to be over 100.000. For each lysate, two to three replicates were measured.

Firefly activity was normalized to the activity of the internal control reporter, including introduced Renilla amounts. Renilla-normalized values were further normalized to positive

control.

Co-Transfection and luciferase assay were carried out six times for each used cell line, three times with MNS16A DNA from one cesium chloride preparation and three times DNA from second cesium chloride preparation was used.

From all six normalized values of each MNS16A VNTR, average values were calculated.

3.3. Statistical evaluation

All statistical analysis were carried out using the statistical programming language R (R Core Team, 2014). P-values greater than 5% were considered statistically significant.

R Core Team (2014). R: A language and environment for statistical computing. R Foundation for Statistical Computing, Vienna, Austria.

3.3.1. MNS16A functional analysis

Descriptive analysis included assessing the distributions of normalized pGL3-values and normalized MNS16A VTNR-values for A-427 and LNCaP cell lines, respectively, by calculating means, standard deviations and distribution plots for each cell line. Differences in mean values were tested using “Welch two-sample t-test” for unequal variances after confirming relevant assumptions.

Relationships between MNS16A-VNTR length and promoter activity were assessed by regression analysis for A427 and LNCaP with MNS16A length as predictor for promoter activity. The shapes of the relationships were investigated by loess smoothing. Depending on the type of relationship, linear, quadratic or piecewise linear regression was applied. The model fits were assessed by diagnostic plots and by measures of explained variance. Significance tests and confidence intervals were derived for regression coefficients and the overall model.

In order to compare promoter activity between cell lines A427 and LNCaP, values were divided by mean pGL3-values. Descriptive statistics and distribution plots were produced for both cell lines. Difference in means was assessed by “Welch two-sample t-test” for unequal variances.

4. Results

4.1. Preparatory experiments

4.1.1. Cloning MNS16A alleles

MNS16A VNTRs were cloned from pCRII-TOPO vector, leading to MNS16A fragment lengths, listed in table 18.

MNS16A	Fragment length
VNTR-364	463nt
VNTR-333	425nt
VNTR-302	394nt
VNTR-274	366nt
VNTR-243	335nt
VNTR-212	274nt

Table 18. MNS16A fragment lengths after cloning VNTRs from pCRII-TOPO vector.

Excised MNS16A fragments were ligated into appropriate pGL3-basic vectors. During ligation, vector controls were performed for each pGL3 vector digestion variant. Each ligation approach was transformed into competent E.Coli cells and plated onto agar plates. pGL3-XhoI/HindIII and pGL3-XhoI/SacI vector control plates showed more than 10 clones, but markedly fewer compared to ligation plates. pGL3-SmaI/SacI vector control plate exhibited only one ligation clone.

Correct insertion of the MNS16A VNTR was validated by the restriction digestion, described in table 2. Figure 3 shows results of agarose gel electrophoresis, performed after restriction digestion. All lanes exhibit DNA bands at approximately 4000bp, representing linearized pGL3-basic vector (4818bp). Clone 1-4 from VNTR-333, VNTR-234, VNTR-302 and VNTR-212 showed correct ligation (Figure 3), verifiable through specific DNA bands at the appropriate size (table 18). Clone 4 from VNTR-364 and clone 1 and 3 from VNTR-274 showed no specific DNA bands at 463bp (VNTR-364) and at 366bp (VNTR-274), respectively indicating no successful ligation. Correct ligation was only detectable in VNTR-364 clone 1-3 and in VNTR-274 clone 2 and 4 (Figure 3).

Clone 1 from VNTR-333, VNTR-243, VNTR-302, VNTR-364 and VNTR-212, and clone 2 from VNTR-274 were further purified by cesium chloride gradient centrifugation.

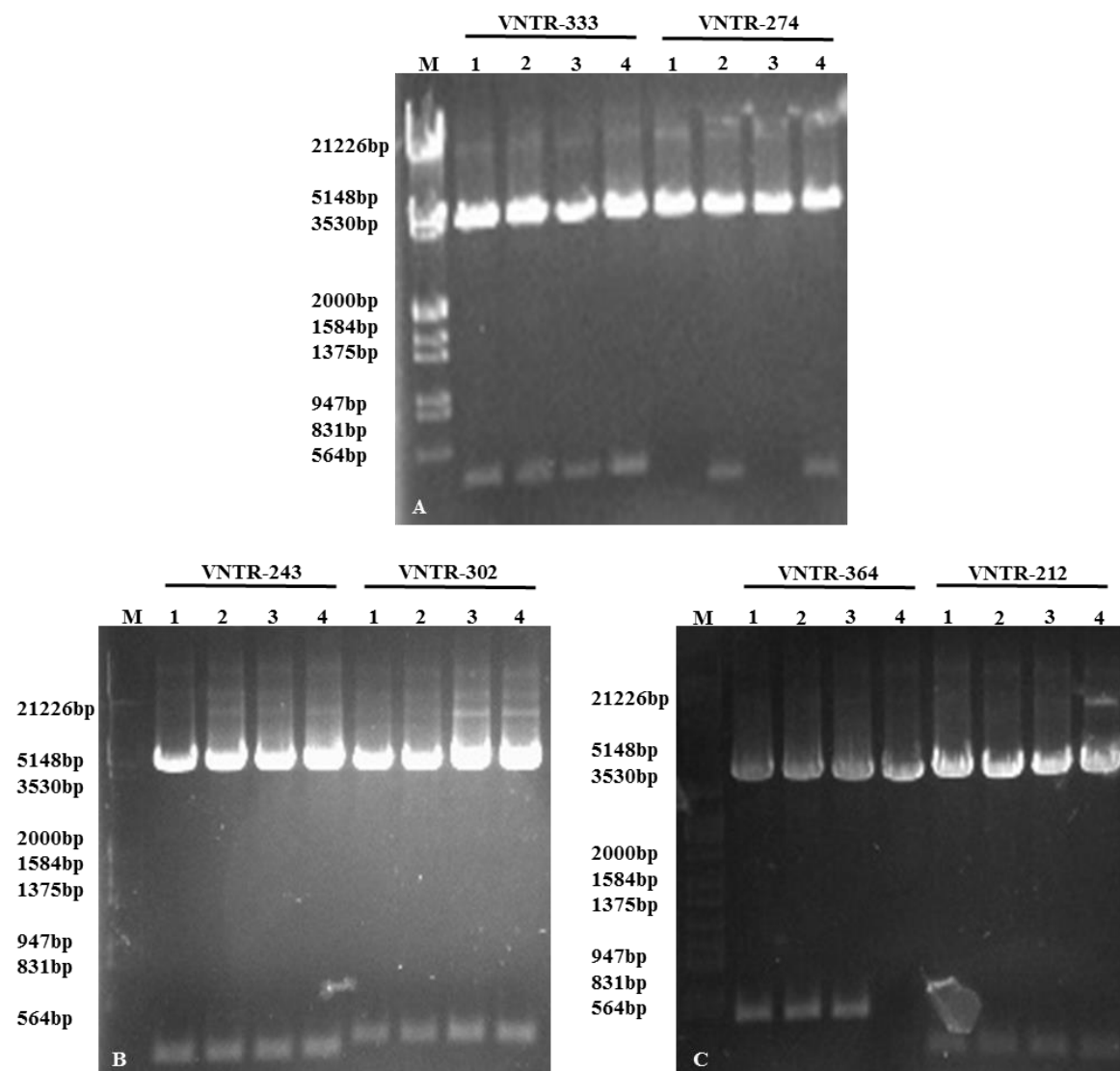


Figure 3. Verifying MNS16A cloning, using restriction digestion and agarose gel electrophoresis. Restriction digestions were performed, using 5µl from each cloned DNA (clone 1-4 from individual MNS16A VNTRs). Resulted DNA fragments were separated in 1.2% agarose gels (A, B, C), by mixing whole digestion approaches with 6xloading buffer (50-100V). Lambda DNA/EcoRI+HindIII Marker 3 was used as length reference (M). DNA bands were detected by staining with ethidium bromide solution and by UV illuminating.

4.1.2. DNA purification by cesium chloride banding

4.1.2.1. First cesium chloride preparation of cloned MNS16A constructs

After cesium chloride density gradient centrifugation, multiple ethanol precipitations, multiple PCI and one chloroform-isoamylalcohol extraction, purified DNAs were dissolved in ddH₂O and DNA concentrations were quantified (table 19).

MNS16A	DNA concentration
VNTR-364	692ng/μl
VNTR-333	708ng/μl
VNTR-302	733ng/μl
VNTR-274	670ng/μl
VNTR-243	922ng/μl
VNTR-212	588ng/μl

Table 19. Quantified MNS16A DNA concentrations.

Restriction digestions were performed (table 2), checking purified MNS16A constructs. Figure 4 shows agarose gels, performed after restriction digestions. At approximately 4900bp, linearized pGL3-vector was visible in each lane. Weak signals for all MNS16A fragments were detectable (Figure 4) at their respective sizes (table 18). Consequently, the correct DNAs were purified.

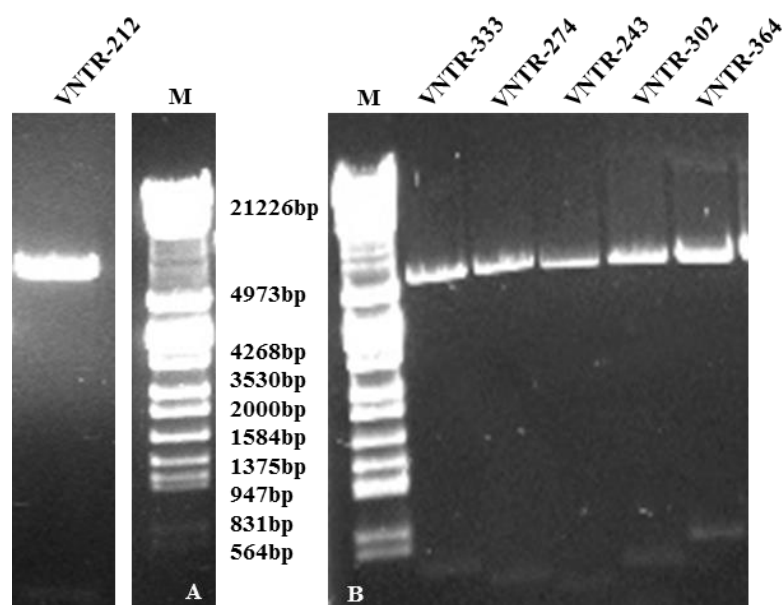


Figure 4. Verifying purified MNS16A constructs, using restriction digestion and agarose gel electrophoresis. 250ng from each MNS16A construct were digested (exception: VNTR-212 with 500ng). 1% (A) and 1.2% (B) agarose gel were used to separate resulted DNA fragments, by mixing whole approaches with 6xLoading Buffer. Lamda DNA/EcoRI+HindIII Marker,³ was used as length standard (M). Ethidium bromide solution and UV light were used for DNA detection. Each cloned MNS16 allele was loaded into one lane.

After restriction digestion, further ethanol precipitation was performed and MNS16A constructs were dissolved in 1xT/E pH7, getting final concentrations of approximately 500ng/μl. Table 20 registers measured concentrations.

MNS16A	DNA concentration
VNTR-364	551ng/μl
VNTR-333	530ng/μl
VNTR-302	529ng/μl
VNTR-274	540ng/μl
VNTR-243	515ng/μl
VNTR-212	545ng/μl

Table 20. Quantified MNS16A DNA concentrations

Probes from each cloned MNS16A VNTR were loaded onto agarose gels, verifying measured DNA concentrations (Figure 5).

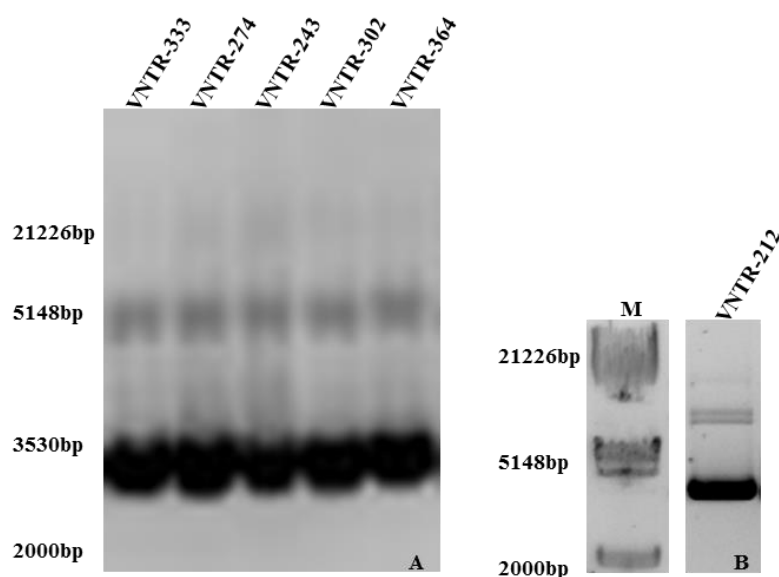


Figure 5. Amount comparison to verify quantified DNA concentrations of the purified MNS16A constructs. 1μl from each cloned MNS16A allele, mixed with T/E pH 7 and 6xLoading Buffer were loaded onto 0.8% agarose gels in different lanes (50-100V). Lambda DNA/EcoRI+HindIII Marker, 3 was used as marker (M). Ethidium bromide solution and UV light made DNA bands visible. Cloned vector sizes: 5214bp (VNTR-333), 5155bp (VNTR-274), 5124bp (VNTR-243), 5183bp (VNTR-302), 5260bp (VNTR-364), 5075bp (VNTR-212).

Amount comparison (Figure 5) exhibited DNA bands at about 5000bp in all lanes, representing nicked/linear pGL3-MNS16A-VNTRs DNA, whereas signals at

approximately 3000/4000bp represent the appropriate supercoiled plasmid DNA. In figure 5-A, all MNS16A constructs had roughly the same signal strengths, indicating to have the same concentrations. Based on this gel (Figure 5-A) and on quantified concentrations (table 20), DNA concentrations of this five MNS16A constructs were estimated at 500ng/μl. Cloned VNTR-212 was loaded onto a distinct gel (Figure 5-B). DNA concentration of VNTR-212 was also estimated at 500ng/μl, according to measured DNA concentration (table 20).

These first CsCl-preparations of cloned MNS16 VNTRs were utilized for luciferase assays in each used cancer cell lines.

4.1.2.2. Second cesium chloride preparation of cloned MNS16A constructs

All cloned MNS16A alleles were prepared a second time, using cesium chloride banding.

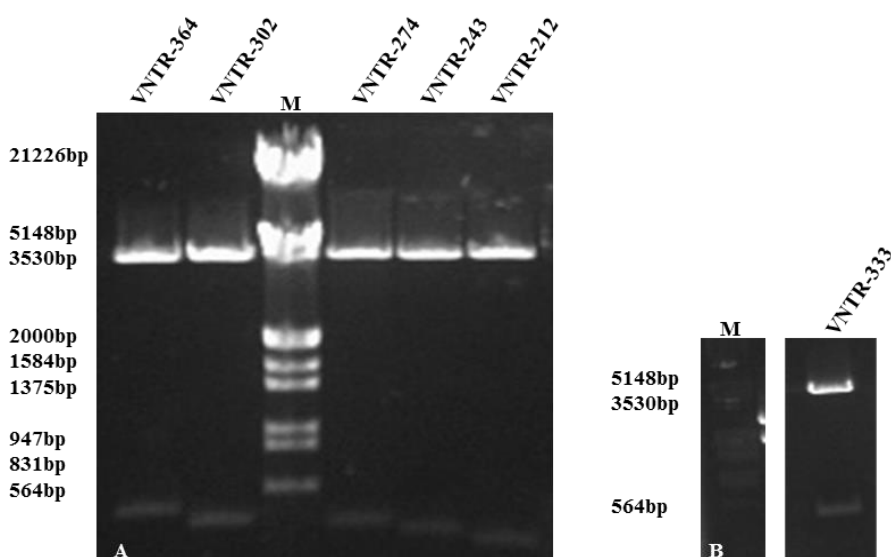


Figure 6. Verifying second round of purified MNS16A constructs, using restriction digestion and agarose gel electrophoresis. Cloned MNS16A alleles were digested, using 500ng from each construct (dissolved in 1xT/E pH 7). VNTR-333 was digested such as described in table 2.2 and fragments (425bp and 4818bp) were separated, using 1% agarose gel (B). Remaining VNTRs were digested, using KpnI and HindIII, and loaded onto 1.2% agarose gel (A). Lambda DNA/EcoRI+HindIII Marker, 3 was used as length standard (M). Ethidium bromide solution and UV-light were used for DNA detection.

KpnI and HindIII produced following digestion patterns: 488bp + 4770bp (VNTR-364), 413bp + 4770bp (VNTR-302), 385bp + 4770bp (VNTR-274), 354bp + 4770bp (VNTR-243) and 305bp + 4770bp (VNTR-212).

After preparation, precipitation and extraction, cloned MNS16A VNTRs were also digested. Resulted fragments were separated on agarose gels (Figure 6). Linearized pGL3-

basic vector was detectable in all six lanes at around 4000bp. In addition, all MNS16A fragments were traceable at their appropriate sizes, as described in figure 6. Hence, it can be affirmed, that correct DNAs were prepared.

MNS16A	DNA concentration
VNTR-364	558ng/μl
VNTR-333	560ng/μl
VNTR-302	550ng/μl
VNTR-274	561ng/μl
VNTR-243	533ng/μl
VNTR-212	546ng/μl

Table 21. Quantified concentrations of cloned MNS16A preparations.

Additionally, two gels were used for amount comparison. VNTR-364, -302 and -212 showed the same signal strength, having the same DNA concentrations (Figure 6). Weak signal strengths were detectable for VNTR-274 and VNTR-243. Compared to the quantified concentrations (table 21), MNS16A concentrations were estimated at 500ng/μl for VNTR-364, -302 and -212 and at 400ng/μl for VNTR-274 and -243.

VNTR-333 construct was loaded onto another gel (Figure 6-B). Due to comparison VNTR-333 signal strength to other probes on the gel (not shown in this picture) and to measured concentration (table 21), VNTR-333 concentration was estimated to 500ng/μl.

Three luciferase assays of each used cell line were performed, utilizing these second MNS16A VNTR preparations.

4.2. Qualitative determination of transfection efficiency of cell lines

Multiple cell lines, listed in table 13, were transfected with pAdlox CFP vector, figuring out those lung and prostate cancer cell lines with best transfection efficiency. Each cell line was transfected, using eight different approaches (Table 3.19), to find the condition, which lead to best transfection efficiency.

4.2.1. Lung cancer cell lines

Among 15 tested lung cancer cell lines (table 13), VL-8, SK-LU-1 and A-427 exhibited best transfection efficiency. Since the measured Firefly activity of the positive control (77.089) of SK-LU-1 was insufficient and the measured Firefly and Renilla activities of VL-8 were near the background noise, these two cell lines were not used for final MNS16A functional analysis. Hence, CFP transfection of only A-427, which was used in final experiments, is reported here.

Figure 7 shows results of pAdlox CFP transfections, using four different test conditions. Although the same cell number (200.000) was seeded in all approaches, the overall cell number in glycerol shock approaches (Figure 7-G-J) was definitely lower, compared to approaches without glycerol shock. Enhanced stress due to glycerol shock may be an explanation. Further, only scattered cells showed fluorescence signals, whereby differences in fluorescence efficiency between 5 (Figure 4.5-J) and 10 μ g (Figure 7-H) pAdlox CFP were not detectable. Hence, glycerol shock seems to be prejudicial to A-427 proliferation and transfection efficiency.

Contrary to glycerol shock positive approaches, glycerol shock negative cells showed better cell proliferation, building almost dense cell layers on day 3 and even on day 2 after transfection (Figure 7-A, C, E). Approaches without glycerol shock also clearly generated more fluorescent cells. A-427 cells, transfected with 10 μ g DNA (Figure 7-B), showed markedly increased fluorescence signals, compared to those cells, transfected with only 5 μ g DNA (Figure 7-F).

Finding correct incubation time between transfection and final experiment, which leads to best transfection efficiency, transfection efficiency between day 2 and 3 were compared for those cells, transfected with 10 μ g pAdlox CFP (glycerol shock negative). 2 days after transfection (Figure 7-D) a clearly lower number of cells, transmitted fluorescence signals, were detectable, compared to cells 3 days after transfection (Figure 7-B).

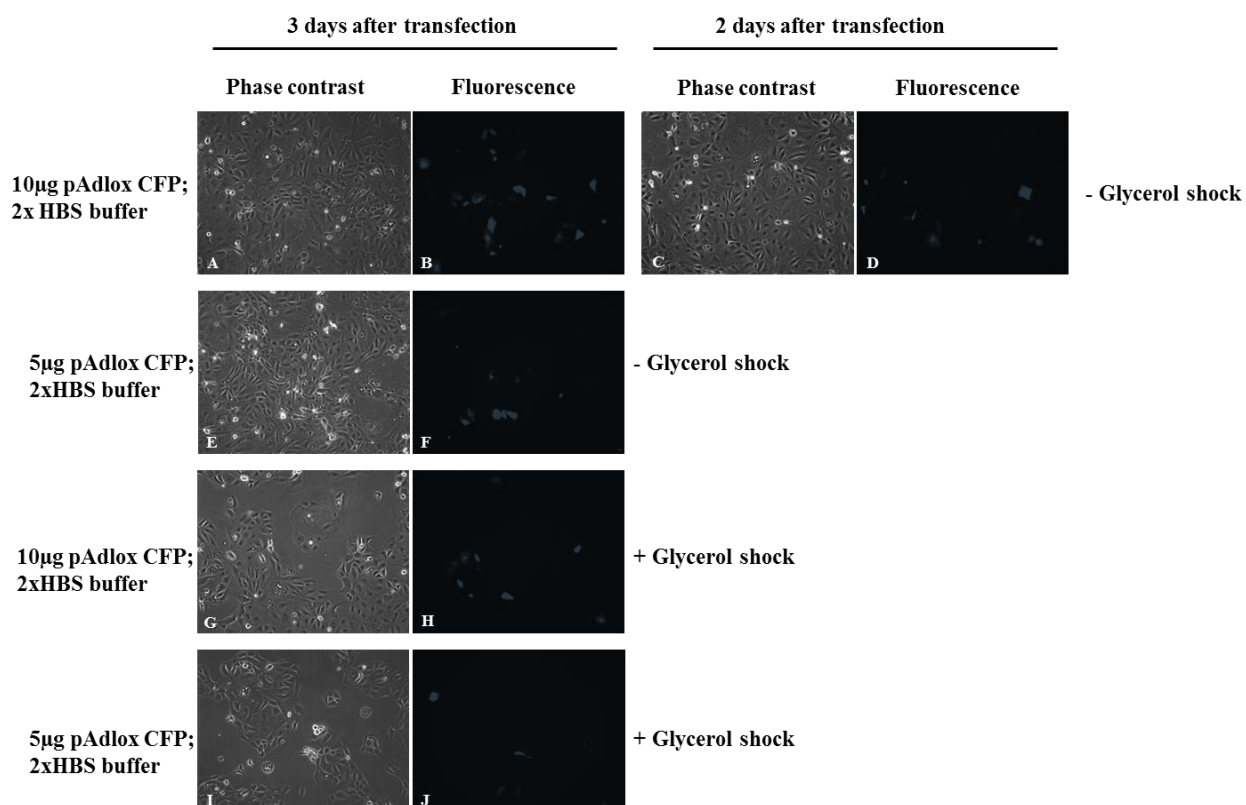


Figure 7. pAdlox CFP transfection of lung cancer cell line A-427 for qualitative determination of transfection efficiency. 200.000 cells were used per approach. Transfections were performed with only 2xHBS buffer, since BBS buffer has not worked well during preceded pAdlox CFP transfections in other cell lines. 5µg (E-F, I-J) as well as 10µg (A-D, G-H) CFP-DNA were used, whereas always one approach was used for glycerol shock (G-J). After transfection, conditioned medium was removed immediately, without 5 minutes incubation. Used reagents (buffer, DNA, water and CaCl₂) were thawed on ice, instead of 25° Celsius in water bath.

Phase contrast (exposure time: 0.5ms) and fluorescence (exposure time: 5000ms) images were taken 2 and 3 days after transfection.

Based on these results, 200.000 (300.000) A-427 cells were transfected with 10µg DNAs without glycerol shock, using 2xHBS buffer. Luciferase assays were performed three days after transfection.

4.2.2. Prostate cancer cell lines

Three prostate cancer cell lines, listed in table 13, were examined for best transfection efficiency. PC-3 as well as LNCaP were found to have high transfection efficiency, but PC-3 was excluded from luciferase experiments, due to too small luciferase signal from positive control (82.435).

Since, LNCaP was the only cell line, used for final experiments, only CFP-transfection results of LNCaP are described.

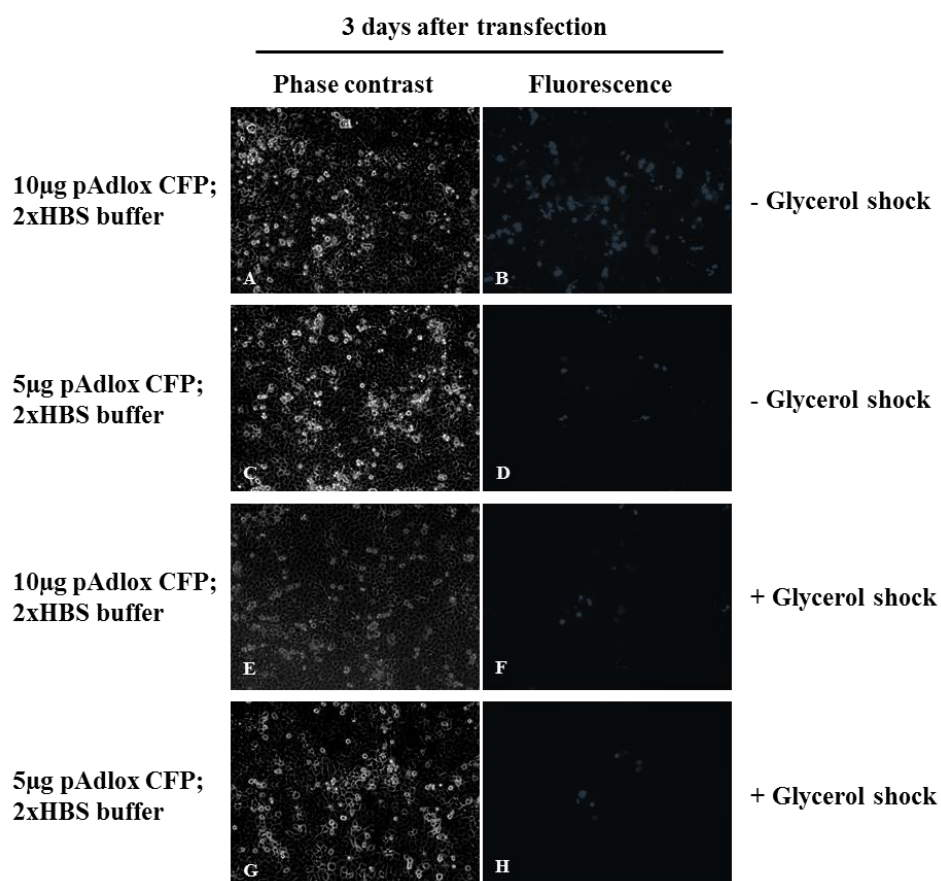


Figure 8. pAdlox CFP transfection of prostate cancer cell line LNCaP for qualitative determination of transfection efficiency. 200.000 cells were used per approach. Transfection were also performed only with 2xHBS buffer. 5µg (C-B, G-H) as well as 10µg (A-B, E-F) pAdlox CFP DNA were used, whereas always one approach was used for glycerol shock (E-H).

Phase contrast (exposure time: 0.5ms) and fluorescence (exposure time: 5000ms) images were taken on day 3 after transfection. On day 2 after transfection, no pictures were taken, because earlier transfections of other cell lines always showed best transfection efficiency on day 3.

All pictures, presented in Figure 8, were taken on day 3 after transfection, showing 100% dense cell layers for all test conditions (Figure 8-A, C, E, G). Consequently, plenty of round, dead LNCaPs, forming cluster of cells, were detectable in all four approaches. Since such circumstances may negatively influence transfection efficiency, 175.000 cells instead of 200.000 cells were seeded for final MNS16A functional analysis.

Both glycerol shock positive approaches (Figure 8-F, H) led to only few countable fluorescent cells (Figure 8-F: 18 cells, Figure 8-H: 8 cells). 10µg CFP-DNA (Figure 8-F) seemed to result in a minimal higher transfection efficiency. However, none of these two conditions reached the efficiency, which was needed for luciferase assays.

Transfecting 5µg pAdlox CFP without glycerol shock (Figure 8-C-D) also resulted in very low transfection efficiency, with only few fluorescent cells compared to the overall cell number. Transfecting 10µg pAdlox CFP without glycerol shock (Figure 8-A-B) resulted in very high transfection efficiency, compared to other test conditions. The whole culture dish was strewn with fluorescent cells. It can be estimated, that, compared to the entire cell number, 60-70% cells transmitted fluorescence signals.

Consequently, 10µg DNAs were transfected into LNCaP cells for MNS16A functional analysis. No glycerol shock was used. Measuring luciferase signals was performed three days after transfection.

4.3. MNS16A functional analysis

4.3.1. MNS16A promoter activity in A-427

Figure 9 exhibits the boxplot diagram from the used lung cancer cell line A-427. The diagram describes single promoter activity values of all six MNS16A VNTRs, measured during luciferase assays.

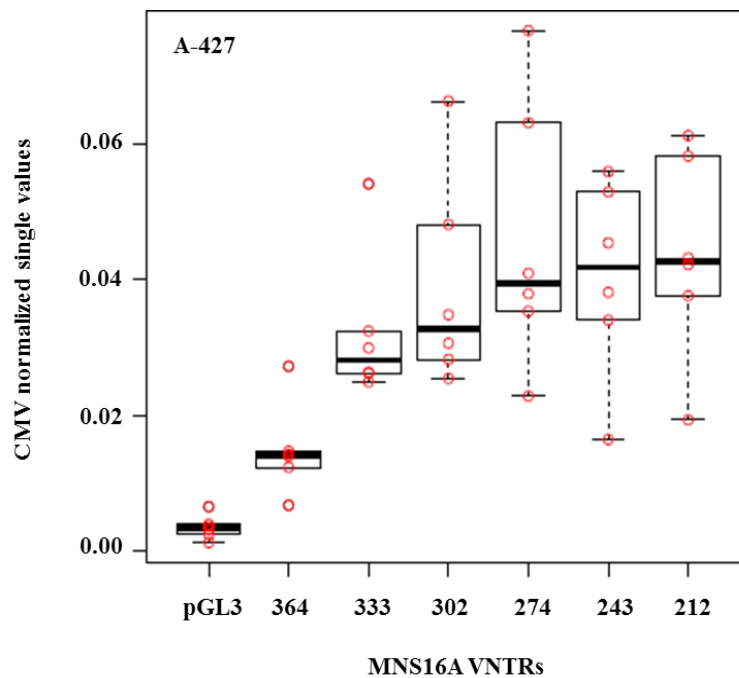


Figure 9. Boxplot diagram of measured values from all six MNS16A VNTRs in the lung cancer cell line A-427.

In A-427 it was clearly shown that measured VNTR-values represented promoter activity. The size of MNS16A VNTRs was significantly higher in contrast to the appropriate negative control values (table 22). This statistically proves that measurements in A-427 were no background noise.

	A-427
Difference of means	-0.0326
T	-11.1334
df	38.6
p-value	1.299x10 ⁻¹³
95% confidence interval	-0.0385; -0.0267

Table 22. Results of „Welch two-sample t-test“, to determine promoter activity of MNS16A constructs in A-427 (compared to negative control).

A significant negative linear relationship between length of MNS16A-VNTR and promoter activity was found for A427 (regression coefficient for MNS16A-VNTR length: -0.0001660, $T = -3.466$, p -value: 0.0015). Visual assessment of the relationship (Figure 10) shows, that the negative trend strengthens between VNTR-302 and VNTR-333. In order to model the changing linear slope, piecewise linear regression with a single breakpoint was estimated. The slope change was predicted between VNTR-302 and VNTR-333, resulting in two regression coefficients of -0.00002678 ($T = 0.362$, p -value = 0.71966) for the left hand side and -0.0005634 ($T = -3.245$, p -value = 0.00269) for the right hand side. Comparing adjusted R^2 -values for model 1 and 2 gives a significant improvement ($p = 0.0238$) of model fit from 0.24 to 0.33 (Figure 10).

Consequently, VNTR-364 has the lowest promoter activity. Although, promoter activity increases strongly to VNTR-302, the MNS16A VNTRs, shorter than VNTR-333, seem to have nearly the same promoter activities. No definite rise in promoter activity from VNTR-302 to VNTR-212 is detectable.

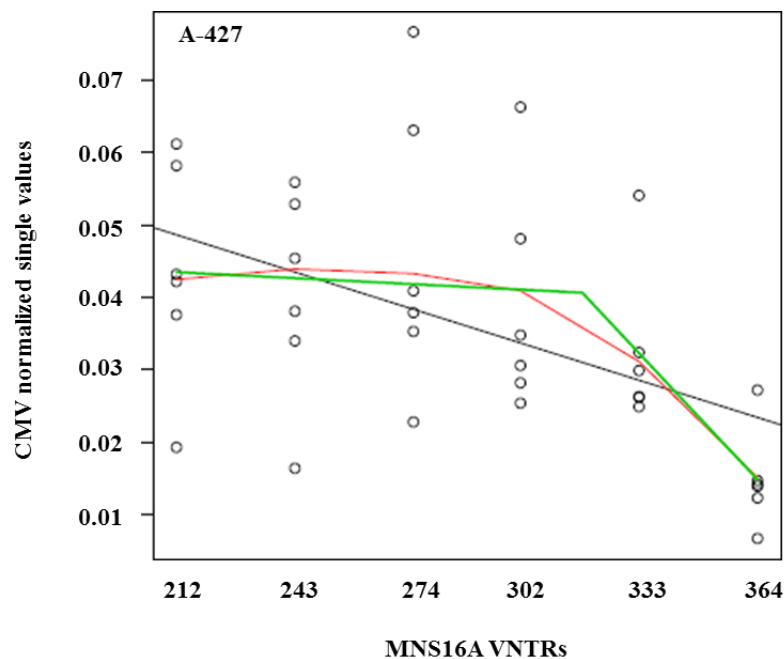


Figure 10. Regression analysis of MNS16A-VNTR promoter activities in A-427.

Single VNTR promoter activities (circles) were plotted onto a dotplot. Linear (black), LOESS (red) and piecewise (green) regressions were performed.

4.3.2. MNS16A promoter activity in LNCaP

The boxplot diagram in figure 11 shows the measured luciferase values, indicating the single promoter activities of all six MNS16A VNTRs of the used prostate cancer cell line LNCaP.

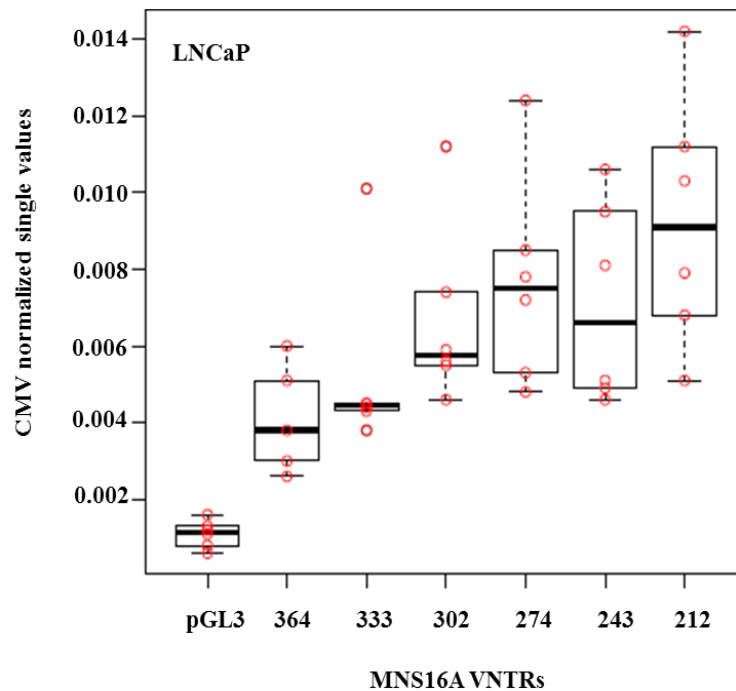


Figure 11. Measured values from all six MNS16A VNTRs from the used prostate cancer cell line LNCaP are represented in this boxplot diagram.

Compared to the appropriate negative control values, the sizes of MNS16A VNTRs were significantly higher (table 23). This statistically proves that measurements were no background noise. Hence, it can be concluded, that in LNCaP measured VNTR-values represented promoter activity.

	LNCaP
Difference of means	-0.0025
T	-11.1288
df	38.3
p-value	1.457x10 ⁻¹³
95% confidence interval	-0.0067; -0.0046

Table 23. This table represents the results of the „Welch two-sample t-test“. Promoter activity of MNS16A constructs of the prostate cancer cell line LNCaP was statistically proven.

Single MNS16A promoter activities, measured in transfected LNCaP cells, are presented in the dotplot diagram (Figure 11). Linear and LOESS regressions were performed (Figure 12).

LNCaP showed a strong negative relationship between length of MNS16A-VNTRs and promoter activity with a slope coefficient of -0.00003034 ($T=-3.702$, $p\text{-value}=0.000777$) and an adjusted R^2 value of 0.27. There was no evidence for a change in regression slope for larger VNTR-values.

Consequently, this shows a continuous rise of promoter activity, with the lowest activity at VNTR-360 and the highest one at VNTR-212. Since, no changes in the slope were detectable, it was concluded that the shorter MNS16A, the higher its promoter activity.

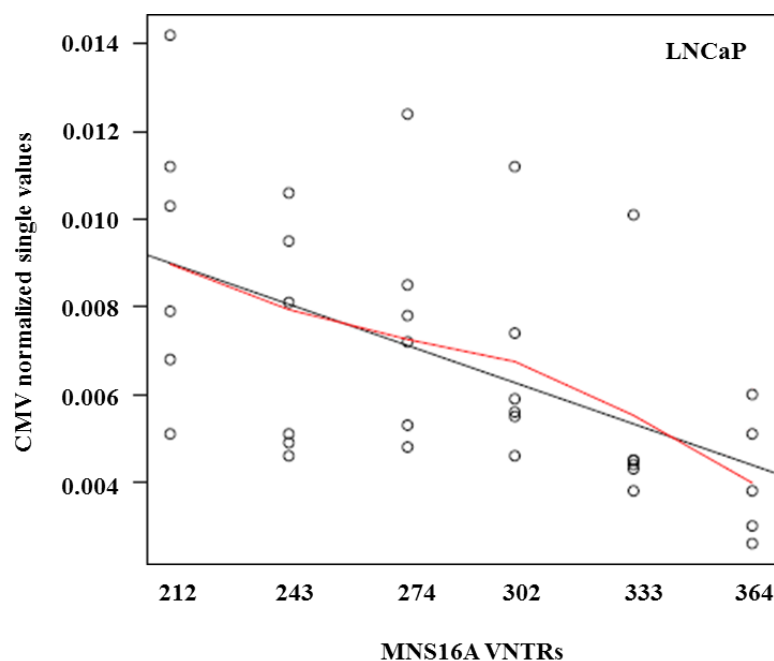


Figure 12. Dotplot presentation of single MNS16A promoter activities (circles) in LNCaP. Linear (black) and LOESS (red) regressions were conducted.

4.3.3. A-427 MNS16A promoter activity compared to LNCaP

Beside MNS16A analysis in A-427 and LNCaP, MNS16A promoter activities were also compared between these two cell lines (Figure 13), to find possible significant differences.

Since pGL3-basic (negative control) values in A-427 are significant higher (p-value: 0.02221) than pGL3-basic values in LNCaP, VNTR-values had to be normalized to the average value of the appropriate pGL3 values for promoter activity comparison.

Despite significant differences in pGL3-basic values between the two cell lines, A-427 exhibited significant higher (p-value: 2.6×10^{-5} ; table 24) MNS16A promoter activities compared to LNCaP.

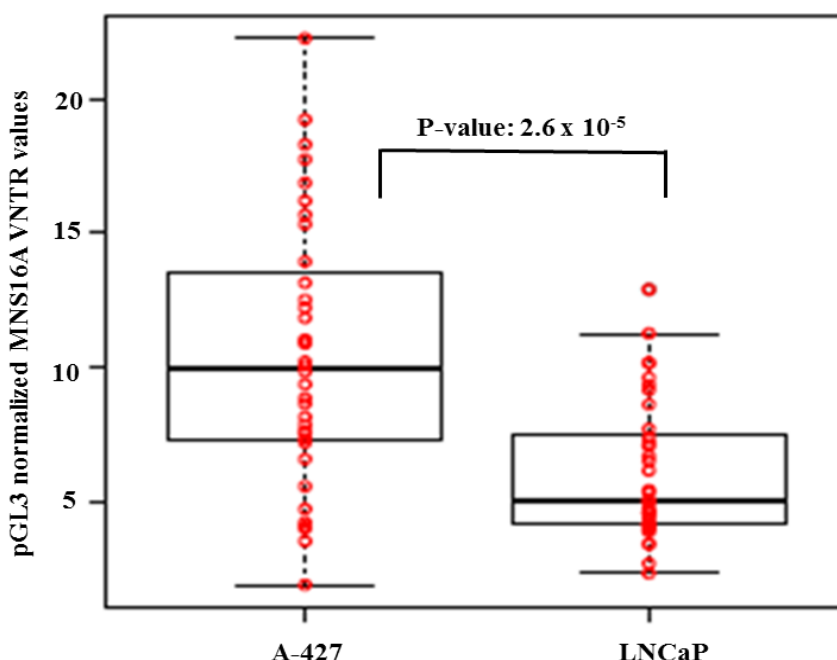


Figure 13. Boxplot diagram of pGL3 normalized MNS16A VNTRs values of A-427 and LNCaP. It represents the statistically significant differences in MNS16A promoter activity between the two cell lines.

	A-427	LNCaP	“Welch two-sample t-test”	
Mean values	10.4453	6.1455	Difference of means	4.299795
Standard deviations	4.9311	2.6201	T	4.6057
			df	53.624
			p-value	2.6×10^{-5}
			95% confidence interval	2.427764; 6.171826

Table 24. Left column exhibits mean values for ratios of promoter activity of A-427 and LNCaP, normalized by corresponding pGL3-values. Right column shows results of “Welch two-sample t-test”, to compare MNS16A promoter activity in both used cell lines.

5. Discussion

In a lung cancer study, Wang et al. (2003) [1] identified a polymorphic tandem repeats minisatellite at the hTERT locus, named MNS16A. In this study, four different MNS16A alleles were identified: VNTR-243, VNTR-274, VNTR-302 and VNTR-333 [1]. Additionally, our group observed a rare fifth MNS16A allele (VNTR-212) in a PC study [3] and a sixth variant (VNTR-364) in a colorectal cancer (CRC) study [2], for the first time. According to their different lengths, all six MNS16A alleles were divided into (S) short (VNTR-212 / 243 / 274) and (L) long (VNTR-302 / 333 / 364) VNTRs, giving rise to three genotypes: SS, SL and LL [1-3].

Wang et al. [1] first identified MNS16A as a potential risk factor in a hospital based case-control lung cancer study. In this study, the LL genotype showed a significantly increased risk for developing NSCLC in a Caucasian and African-American population [1]. A glioblastoma multiforme (GBM) study from Wang et al. [121] associated the LL genotype with the shortest survival time in a non-Hispanic white patient population [121]. Jin et al. [122] identified VNTR-243 allele and VNTR-243 containing genotypes as risk factors for lung cancer in a Korean patient population. Carpentier et al. [123] found the SL and SS genotypes to be associated with increased risk of malignant gliomas in a Caucasian population [123]. In a hospital based case-control CRC study, our group [2] detected an association between the VNTR-274 allele and the significantly increased CRC risk in a Caucasian patient population [2]. Wang et al. [124] detected an association between the SS genotype and a shorter survival in stage I NSCLC of non-Hispanic white patients [124]. In a GBM study Andersson et al. [125] showed an association of the SS genotype with the shortest median survival in a north-European population [125].

Additionally, Andersson et al. [125] detected an association of the LL genotype with the longest median survival in GBM patients [125]. Our group [3] investigated MNS16A variants in context to PC, for the first time. Interestingly, in a Caucasian patient population this study exhibited a significantly reduced PC risk for men older than 70 years, concerning VNTR-274 and the 274/302 genotype [3]. In a case-control nasopharyngeal carcinoma (NPC) study, Zhang et al. [126] confirmed these results in a Chinese population [126]. In the lung cancer study from Jin et al. [122] the VNTR-243 covering genotypes were associated with significantly longer overall survival in a Korean population [122]. In the GBM study from Wang et al. [121] the SS genotype was associated with the longest

survival time [121].

These molecular epidemiological studies led to partly conflicting results, regarding both cancer risk and survival. Contradictory results are not only present among different malignancies, but also within studies of the same cancer type [1-3, 121-127]. Hofer et al. [3] explains the inconsistent results among different malignancies through discrepancies in the molecular mechanism of tumorigenesis [3]. Additional factors, as distinct tumour stages and patient's age in the different studies, may influence these conflicting results [1-3, 121-127]. In a lung cancer study, Wang et al. [124] found different associations between MNS16A alleles and survival, depending on tumour stage [124], whereas a PC study [3] found an association between a MNS16A allele and decreased PC risk, depending on the patient's age [3].

Otherwise, the inconsistent results of MNS16A epidemiological studies [1-3, 121-127] may emerge due to discrepancies through a selection bias, distinct study designs and genotyping methods and through different genotype frequencies in the various investigated ethnicities [3].

Since MNS16A is situated downstream of the hTERT gene, in the promoter region of the antisense hTERT transcript, Wang et al. [1] measured potential functionality of the wild-type allele VNTR-302 and the shorter allele VNTR-243. Based on the observation that both alleles exhibited promoter activity and that VNTR-243 distinctly showed higher promoter activity than VNTR-302, it was argued that MNS16A promoter activity depends on the allele length. Moreover, a repressive function of MNS16A for hTERT antisense RNA transcription and a negative influence on hTERT expression were postulated [1].

This study is the first, which analysed functionality of all six known MNS16A VNTRs in a lung cancer cell line. The study approves the results from Wang et al [1], that VNTR-302, VNTR-243 contain promoter activity. Further, in our study promoter activity was also detected for the remaining four VNTRs in a lung cancer cell line for the first time. Wang's conclusion, that promoter activity is inversely correlated to MNS16A length [1], could be only observed for the L alleles in our used lung cancer cell line A-427. In our study, a significant increase of promoter activity was detectable from VNTR-364 to VNTR-302. The promoter activity, concerning the remaining shorter alleles, appears to be not significantly increasing. Wang et al. [1] observed a distinct increase of promoter activity

from the wild-type allele VNTR-302 to the shorter allele VNTR-243 [1]. Although, in our study an increase of promoter activity between these two alleles was observed, no significance was detected.

The results, concerning lung cancer MNS16A functionality in this study compared to Wang et al. [1], are indicative of a functional heterogeneity of MNS16A in lung cancer. Due to the usage of the lung cancer cell line A-427 in our and H1299 in Wang's study [1], MNS16A functionality seems to be cell line specific [1]. Both epithelial lung cancer cell lines were derived from male Caucasians, suffering from lung carcinoma. However, the cell line A-427 in our study was isolated from primary lung tumour, whereas H1299 was derived from lymph node metastasis of the lung [128]. Hence, a dependence of MNS16A functionality on tumour progression can be assumed and consequently leading to distinct results, comparing the two different lung cancer cell lines [1]. Additionally, the appropriate patient, from whom H1299 was isolated, was treated with radiation therapy before cell line establishment [128], also probably affecting MNS16A promoter activity [1].

Moreover, for the first time promoter activity of all six known MNS16A VNTRs was additionally detected in the prostate cancer cell line LNCaP. The results show an inverse correlation between promoter activity and MNS16A length.

Beside the difference in the correlation between MNS16A length and promoter activity in the used lung and prostate cancer cell lines, also an overall higher promoter activity was detectable in A-427 compared to LNCaP. Hence, a tissue specificity of MNS16A can be observed. Additionally, the used epithelial prostate cancer cell line LNCaP, derived from a 50 years old male Caucasian, was isolated from supraclavicular lymph node metastasis of the prostate [128]. Since A-427 was isolated from a primary lung tumour [128], a tumour stage dependence could explain the different results between LNCaP and A-427, too.

Due to the results, concerning MNS16A functionality in the two used cell lines, studying MNS16A promoter activity in additional PC and lung cancer cell lines would be beneficial.

In multiple studies, concerning lung [122], breast [127] and malignant glioma [123] cancers, VNTR-243 or VNTR-243 containing genotypes were associated with increased cancer risk compared to the wild-type allele [122, 123, 127]. Jin et al. [122] explained these results through the behaviour of the MNS16A functionality and the antisense hTERT transcript [1, 122]. Since VNTR-243 is shorter than VNTR-302, it has higher promoter

activity, according to Wang et al. [1] and to the PC cell line results of this study. This may leads to higher levels of antisense hTERT RNA expression [1]. Since antisense hTERT transcripts probably negatively regulates hTERT expression [1], VNTR-243 leads to lower hTERT expression, which positively influences tumorigenesis [122], whereas in a NPC study lower hTERT expression also influences tumorigenesis negatively [126]. Additionally, VNTR-243 was also associated with increased survival in a lung cancer study, which was explained due to distinct roles of telomerase in different tumour stages [122]. Nevertheless, these results [122, 123, 126, 127] are in line with the finding, that MNS16A functionality is inversely correlated to the number of core tandem repeats [1]. However, in other epidemiological studies, long MNS16A alleles [1] as well as medium-length VNTRs [2] were associated with increased cancer risk. These results [1, 2] cannot be explained through MNS16A functionality's behaviour, observed in LNCaP.

Since the longest (VNTR-364) and shortest (VNTR-212) known alleles have the lowest and partly the highest promoter activity, molecular epidemiological studies, concerning these two alleles in context of distinct malignancies, would be interesting. However, in all realized molecular epidemiological studies, these two alleles were not included, since they were unknown at the time of publication or excluded because of very rare occurrence [1-3, 121-127].

Due to the supposed tissue specificity of the MNS16A promoter activity, it would be advisable to explain epidemiological results by MNS16A functionality, observed in appropriate cancer cell lines.

It is well established, that VNTRs are associated with the susceptibility of various diseases and that they partly display functionality (reviewed in [129]). VNTR elements, which are located in the 3' untranslated regions are known to effect translation [129, 130], whereas VNTRs in coding sequences modify protein structure and consequently protein activity [129, 131, 132]. Moreover, various VNTR sequences, located in the 5' control region, influence gene expression through transcriptional regulation (reviewed in [129]), such as MNS16A [1].

Like MNS16A [1], various VNTR elements in different promoter regions exhibit similar sequence structures and have a negative influence on transcription [133-136], as VNTR sequences in the RHOB promoter [133], in the cystatin B promoter [134], in the secretin

promoter [135] and in the promoter of a gene on chromosome 11p15 [136].

The RHOB promoter minisatellite lead to four different alleles with distinct numbers of a 34bp tandem repeat element. The function does not depend on the length of the VNTR sequence, which is comparable to MNS16A functionality in the lung cancer cell line A-427. However, the precise mechanism of its repression function is not known [133].

The repressive minisatellite of the cystatin B gene promoter showed a decreased transcription with the mounting number of dodecamer repetitive units [134], comparable with the secretin promoter minisatellite [135] as well as with MNS16A functionality in the PC cell line. The behaviour of the cystatin B promoter minisatellite was explained through the disruption of the promoter by the increasing number of tandem repeats [134], whereas also transcription factors binding to these two minisatellite were observed [134, 135].

The minisatellite in the promoter of a gene on chromosome 11p15, leading to four different alleles with distinct numbers of a 38bp repetitive unit, also showed an inverse correlation between the length of the sequence and promoter activity. It is speculated, that this minisatellite also contains transcription factor binding sites, which modulate the efficiency of the transcription repression, dependent on the number of the tandem repeats [136].

Unlike MNS16A [1], several promoter VNTR sequences were found to enhance promoter activity [137-139], as the VNTR elements in the prostacyclin synthase promoter [138]. This functional VNTR polymorphism, containing different numbers of 9bp tandem repeats elements, results into four different alleles. A dependence of functionality from the number of the repetitive sequences was detected, whereas the greatest promoter activity was linked to the longest allele, also showing the highest quantity of Sp-1 binding sites [138].

Interestingly, functionality of most of these VNTR elements was attempted to explain through binding of diverse transcription factors to the repetitive units [134-136, 138]. This explanation may also apply to MNS16A functionality, making the transcription factor GATA-1, which binds to the CAT trinucleotide insertion of the longer MNS16A tandem repeat [1], to a promising candidate, responsible for the MNS16A behaviour in different cancer cell lines. Hence, investigations, concerning the associations of GATA and possible other transcription factors to MNS16A functionality, are of particular importance.

The GATA transcription factor family is composed of six known members, named GATA-1 to GATA-6. All GATA factors exhibit a highly conserved DNA binding domain,

recognizing the characteristic A/T GATA A/G sequence. These factors, distinctly distributed over many tissues, are involved in the regulation of the cell cycle and cell survival, controlling cellular and distinct tissue development [140]. Aberrations of the different GATA factors, such as expression silencing, are known to be involved in various human malignancies [140], including lung [141] and colorectal [142] cancer.

Since Wang et al. [1] *in silico* identified the 26bp core tandem repeats as a binding site for GATA-1, the GATA family is a promising factor, which may be involved in modulating the MNS16A functionality [1]. Interestingly, GATA family expression profiles, extracted from the Gene Expression Omnibus (GEO) database [143], showed low GATA-1 expression in lung (GSE3141) [144] as well as in prostate (GSE6956) [145] tumours. Additionally, GATA-3 and GATA-6 in lung [143, 144] and GATA-2 in prostate [143, 145] tumours exhibit distinct higher expression levels than GATA-1. Consequently, these factors are probably more important in regulating MNS16A functionality, than GATA-1.

Concerning MNS16A functionality in the PC cell line, it is shown, that with increasing MNS16A length and decreasing promoter activity, the number of the GATA binding sites increases. Consequently, a repressive function of the GATA transcription factor is expected. So far, only an activator function for GATA-2 [146], mainly expressed in prostate tumours [143, 145], is known. Hence, the absence of other GATA transcription factors [143, 145] or the involvement of other transcription factor families may play a role in regulating MNS16A functionality, too.

The exact mechanism, in which the promising GATA transcription factors influence functionality, has to be further clarified. Hence, additional *in vitro* and *in vivo* analysis, concerning the GATA transcription factor family, have to be performed in lung and prostate cancer cell lines.

The MNS16A biological functionality has to be better clarified, before it is used as biomarker in different malignancies. Since functionality is cell line specific [1] and it is possible, that it is influenced by tissue-, tumour stage- [124, 128] and age-specific [3] factors, MNS16A functionality has to be further investigated in additional prostate and lung cancer cell lines, considering these influencing factors. Due to the possible tissue-specificity, showing MNS16A functionality in cell lines, corresponding to the molecular

epidemiological studies, would lead to a better understand of those inconsistent results [1-3, 121-127].

Further, MNS16A promoter activity not only depends on the number of core tandem repeats, but also on specific factors, as GATA transcription factor [1]. Consequently, investigations concerning GATA transcription factor family may clarify differences of MNS16A functionality among diverse cancer cell lines. However, other transcription factor families have to be considered to influence MNS16A promoter activity, too.

The influence of MNS16A alleles on the hTERT antisense transcript levels in different tissues/cell lines and the precise mechanism of regulating hTERT expression through the antisense transcript are also important to investigate [1].

All these points may lead to a better and precise understanding on the influence of MNS16A in tumorigenesis of distinct malignancies.

References

1. Wang, L., et al., *Association of a functional tandem repeats in the downstream of human telomerase gene and lung cancer*. *Oncogene*, 2003. **22**(46): p. 7123-9.
2. Hofer, P., et al., *MNS16A tandem repeats minisatellite of human telomerase gene: a risk factor for colorectal cancer*. *Carcinogenesis*, 2011. **32**(6): p. 866-71.
3. Hofer, P., et al., *MNS16A tandem repeat minisatellite of human telomerase gene and prostate cancer susceptibility*. *Mutagenesis*, 2013. **28**(3): p. 301-6.
4. Ferlay, J., et al., *Cancer incidence and mortality worldwide: Sources, methods and major patterns in GLOBOCAN 2012*. *Int J Cancer*, 2014.
5. Austria, S. *Krebsinzidenz und Krebsmortalität in Österreich*. 2014 23.10.2014]; Available from: http://www.statistik.at/web_de/statistiken/gesundheit/krebserkrankungen/prostata/index.html.
6. Whittemore, A.S., et al., *Family history and prostate cancer risk in black, white, and Asian men in the United States and Canada*. *Am J Epidemiol*, 1995. **141**(8): p. 732-40.
7. Hayes, R.B., et al., *Prostate cancer risk in U.S. blacks and whites with a family history of cancer*. *Int J Cancer*, 1995. **60**(3): p. 361-4.
8. Schaid, D.J., *The complex genetic epidemiology of prostate cancer*. *Hum Mol Genet*, 2004. **13 Spec No 1**: p. R103-21.
9. Hsing, A.W. and S.S. Devesa, *Trends and patterns of prostate cancer: what do they suggest?* *Epidemiol Rev*, 2001. **23**(1): p. 3-13.
10. Nakagawa, H., et al., *Prostate cancer genomics, biology, and risk assessment through genome-wide association studies*. *Cancer Sci*, 2012. **103**(4): p. 607-13.
11. Al Olama, A.A., et al., *Multiple loci on 8q24 associated with prostate cancer susceptibility*. *Nat Genet*, 2009. **41**(10): p. 1058-60.
12. Amundadottir, L.T., et al., *A common variant associated with prostate cancer in European and African populations*. *Nat Genet*, 2006. **38**(6): p. 652-8.
13. Yeager, M., et al., *Genome-wide association study of prostate cancer identifies a second risk locus at 8q24*. *Nat Genet*, 2007. **39**(5): p. 645-9.
14. Gudmundsson, J., et al., *Genome-wide association study identifies a second prostate cancer susceptibility variant at 8q24*. *Nat Genet*, 2007. **39**(5): p. 631-7.
15. Eeles, R.A., et al., *Identification of seven new prostate cancer susceptibility loci through a genome-wide association study*. *Nat Genet*, 2009. **41**(10): p. 1116-21.
16. Eeles, R.A., et al., *Multiple newly identified loci associated with prostate cancer susceptibility*. *Nat Genet*, 2008. **40**(3): p. 316-21.
17. Gudmundsson, J., et al., *Genome-wide association and replication studies identify four variants associated with prostate cancer susceptibility*. *Nat Genet*, 2009. **41**(10): p. 1122-6.
18. Gudmundsson, J., et al., *Common sequence variants on 2p15 and Xp11.22 confer susceptibility to prostate cancer*. *Nat Genet*, 2008. **40**(3): p. 281-3.
19. Gudmundsson, J., et al., *Two variants on chromosome 17 confer prostate cancer risk, and the one in TCF2 protects against type 2 diabetes*. *Nat Genet*, 2007. **39**(8): p. 977-83.
20. Haiman, C.A., et al., *Genome-wide association study of prostate cancer in men of African ancestry identifies a susceptibility locus at 17q21*. *Nat Genet*, 2011. **43**(6): p. 570-3.
21. Kote-Jarai, Z., et al., *Seven prostate cancer susceptibility loci identified by a multi-stage genome-wide association study*. *Nat Genet*, 2011. **43**(8): p. 785-91.
22. Schumacher, F.R., et al., *Genome-wide association study identifies new prostate cancer susceptibility loci*. *Hum Mol Genet*, 2011. **20**(19): p. 3867-75.

23. Sun, J., et al., *Evidence for two independent prostate cancer risk-associated loci in the HNF1B gene at 17q12*. Nat Genet, 2008. **40**(10): p. 1153-5.
24. Takata, R., et al., *Genome-wide association study identifies five new susceptibility loci for prostate cancer in the Japanese population*. Nat Genet, 2010. **42**(9): p. 751-4.
25. Thomas, G., et al., *Multiple loci identified in a genome-wide association study of prostate cancer*. Nat Genet, 2008. **40**(3): p. 310-5.
26. Duggan, D., et al., *Two genome-wide association studies of aggressive prostate cancer implicate putative prostate tumor suppressor gene DAB2IP*. J Natl Cancer Inst, 2007. **99**(24): p. 1836-44.
27. Akamatsu, S., et al., *Common variants at 11q12, 10q26 and 3p11.2 are associated with prostate cancer susceptibility in Japanese*. Nat Genet, 2012. **44**(4): p. 426-9, s1.
28. Xu, J., et al., *Genome-wide association study in Chinese men identifies two new prostate cancer risk loci at 9q31.2 and 19q13.4*. Nat Genet, 2012. **44**(11): p. 1231-5.
29. Eeles, R.A., et al., *Identification of 23 new prostate cancer susceptibility loci using the iCOGS custom genotyping array*. Nat Genet, 2013. **45**(4): p. 385-91, 391e1-2.
30. Amin Al Olama, A., et al., *A meta-analysis of genome-wide association studies to identify prostate cancer susceptibility loci associated with aggressive and non-aggressive disease*. Hum Mol Genet, 2013. **22**(2): p. 408-15.
31. Eeles, R., et al., *The genetic epidemiology of prostate cancer and its clinical implications*. Nat Rev Urol, 2014. **11**(1): p. 18-31.
32. Ahmadiyeh, N., et al., *8q24 prostate, breast, and colon cancer risk loci show tissue-specific long-range interaction with MYC*. Proc Natl Acad Sci U S A, 2010. **107**(21): p. 9742-6.
33. Haiman, C.A., et al., *Multiple regions within 8q24 independently affect risk for prostate cancer*. Nat Genet, 2007. **39**(5): p. 638-44.
34. Yeager, M., et al., *Identification of a new prostate cancer susceptibility locus on chromosome 8q24*. Nat Genet, 2009. **41**(10): p. 1055-7.
35. Kote-Jarai, Z., et al., *Mutation analysis of the MSMB gene in familial prostate cancer*. Br J Cancer, 2010. **102**(2): p. 414-8.
36. Whitaker, H.C., et al., *The rs10993994 risk allele for prostate cancer results in clinically relevant changes in microseminoprotein-beta expression in tissue and urine*. PLoS One, 2010. **5**(10): p. e13363.
37. Freedman, M.L., et al., *Principles for the post-GWAS functional characterization of cancer risk loci*. Nat Genet, 2011. **43**(6): p. 513-8.
38. Albertsen, P.C., *Treatment of localized prostate cancer: when is active surveillance appropriate?* Nat Rev Clin Oncol, 2010. **7**(7): p. 394-400.
39. Cheng, I., et al., *Prostate cancer susceptibility variants confer increased risk of disease progression*. Cancer Epidemiol Biomarkers Prev, 2010. **19**(9): p. 2124-32.
40. Cussenot, O., et al., *Effect of genetic variability within 8q24 on aggressiveness patterns at diagnosis and familial status of prostate cancer*. Clin Cancer Res, 2008. **14**(17): p. 5635-9.
41. Helfand, B.T., et al., *Prostate cancer risk alleles significantly improve disease detection and are associated with aggressive features in patients with a "normal" prostate specific antigen and digital rectal examination*. Prostate, 2011. **71**(4): p. 394-402.
42. Xu, J., et al., *Inherited genetic variant predisposes to aggressive but not indolent prostate cancer*. Proc Natl Acad Sci U S A, 2010. **107**(5): p. 2136-40.
43. Statistik, A. *Krebsinzidenz und Krebsmortalität in Österreich 2014*. 23.10.2014]; Available from: http://www.statistik.at/web_de/statistiken/gesundheit/krebserkrankungen/luftroehre_bronchien_lunge/index.html.
44. Ridge, C.A., A.M. McErlean, and M.S. Ginsberg, *Epidemiology of lung cancer*. Semin Intervent Radiol, 2013. **30**(2): p. 93-8.

45. SEER; Surveillance, Epidemiology, and End Results Program [cited 2014 23.07.2015]; Available from: <http://seer.cancer.gov/statfacts/html/lungb.html>.
46. Neuberger, J.S. and R.W. Field, *Occupation and lung cancer in nonsmokers*. Rev Environ Health, 2003. **18**(4): p. 251-67.
47. Engels, E.A., et al., *Cancer risk in people infected with human immunodeficiency virus in the United States*. Int J Cancer, 2008. **123**(1): p. 187-94.
48. Doll, R. and A.B. Hill, *A study of the aetiology of carcinoma of the lung*. Br Med J, 1952. **2**(4797): p. 1271-86.
49. Schwartz, A.G., et al., *The molecular epidemiology of lung cancer*. Carcinogenesis, 2007. **28**(3): p. 507-18.
50. Hammond, E.C. and H. Seidman, *Smoking and cancer in the United States*. Prev Med, 1980. **9**(2): p. 169-74.
51. Mattson, M.E., E.S. Pollack, and J.W. Cullen, *What are the odds that smoking will kill you?* Am J Public Health, 1987. **77**(4): p. 425-31.
52. Larsen, J.E. and J.D. Minna, *Molecular biology of lung cancer: clinical implications*. Clin Chest Med, 2011. **32**(4): p. 703-40.
53. Marshall, A.L. and D.C. Christiani, *Genetic susceptibility to lung cancer--light at the end of the tunnel?* Carcinogenesis, 2013. **34**(3): p. 487-502.
54. Bailey-Wilson, J.E., et al., *A major lung cancer susceptibility locus maps to chromosome 6q23-25*. Am J Hum Genet, 2004. **75**(3): p. 460-74.
55. Amos, C.I., et al., *A susceptibility locus on chromosome 6q greatly increases lung cancer risk among light and never smokers*. Cancer Res, 2010. **70**(6): p. 2359-67.
56. You, M., et al., *Fine mapping of chromosome 6q23-25 region in familial lung cancer families reveals RGS17 as a likely candidate gene*. Clin Cancer Res, 2009. **15**(8): p. 2666-74.
57. Amos, C.I., et al., *Genome-wide association scan of tag SNPs identifies a susceptibility locus for lung cancer at 15q25.1*. Nat Genet, 2008. **40**(5): p. 616-22.
58. Hung, R.J., et al., *A susceptibility locus for lung cancer maps to nicotinic acetylcholine receptor subunit genes on 15q25*. Nature, 2008. **452**(7187): p. 633-7.
59. Thorgeirsson, T.E., et al., *A variant associated with nicotine dependence, lung cancer and peripheral arterial disease*. Nature, 2008. **452**(7187): p. 638-42.
60. Wang, Y., et al., *Common 5p15.33 and 6p21.33 variants influence lung cancer risk*. Nat Genet, 2008. **40**(12): p. 1407-9.
61. Broderick, P., et al., *Deciphering the impact of common genetic variation on lung cancer risk: a genome-wide association study*. Cancer Res, 2009. **69**(16): p. 6633-41.
62. Rudd, M.F., et al., *Variants in the GH-IGF axis confer susceptibility to lung cancer*. Genome Res, 2006. **16**(6): p. 693-701.
63. Bryce, L.A., et al., *Mapping of the gene for the human telomerase reverse transcriptase, hTERT, to chromosome 5p15.33 by fluorescence in situ hybridization*. Neoplasia, 2000. **2**(3): p. 197-201.
64. McKay, J.D., et al., *Lung cancer susceptibility locus at 5p15.33*. Nat Genet, 2008. **40**(12): p. 1404-6.
65. Rafnar, T., et al., *Sequence variants at the TERT-CLPTM1L locus associate with many cancer types*. Nat Genet, 2009. **41**(2): p. 221-7.
66. Blackburn, E.H., *Switching and signaling at the telomere*. Cell, 2001. **106**(6): p. 661-73.
67. Brown, W.R., et al., *Structure and polymorphism of human telomere-associated DNA*. Cell, 1990. **63**(1): p. 119-32.
68. Moyzis, R.K., et al., *A highly conserved repetitive DNA sequence, (TTAGGG)_n, present at the telomeres of human chromosomes*. Proceedings of the National Academy of Sciences, 1988. **85**(18): p. 6622-6626.

69. de Lange, T., *Shelterin: the protein complex that shapes and safeguards human telomeres*. Genes Dev, 2005. **19**(18): p. 2100-10.
70. Blackburn, E.H., *Structure and function of telomeres*. Nature, 1991. **350**(6319): p. 569-73.
71. de Lange, T., *How telomeres solve the end-protection problem*. Science, 2009. **326**(5955): p. 948-52.
72. Griffith, J.D., et al., *Mammalian telomeres end in a large duplex loop*. Cell, 1999. **97**(4): p. 503-14.
73. Harley, C.B., A.B. Futcher, and C.W. Greider, *Telomeres shorten during ageing of human fibroblasts*. Nature, 1990. **345**(6274): p. 458-60.
74. Hastie, N.D., et al., *Telomere reduction in human colorectal carcinoma and with ageing*. Nature, 1990. **346**(6287): p. 866-8.
75. Weinberg, R.A., *The biology of Cancer*. 2014, Garland Science. p. 391-437.
76. Cifuentes-Rojas, C. and D.E. Shippen, *Telomerase regulation*. Mutat Res, 2012. **730**(1-2): p. 20-7.
77. Lu, W., et al., *Telomeres-structure, function, and regulation*. Exp Cell Res, 2013. **319**(2): p. 133-41.
78. Greider, C.W. and E.H. Blackburn, *Identification of a specific telomere terminal transferase activity in Tetrahymena extracts*. Cell, 1985. **43**(2 Pt 1): p. 405-13.
79. Daniel, M., G.W. Peek, and T.O. Tollefsbol, *Regulation of the human catalytic subunit of telomerase (hTERT)*. Gene, 2012. **498**(2): p. 135-46.
80. Mitchell, J.R., E. Wood, and K. Collins, *A telomerase component is defective in the human disease dyskeratosis congenita*. Nature, 1999. **402**(6761): p. 551-5.
81. Pogacic, V., F. Dragon, and W. Filipowicz, *Human H/ACA small nucleolar RNPs and telomerase share evolutionarily conserved proteins NHP2 and NOP10*. Mol Cell Biol, 2000. **20**(23): p. 9028-40.
82. Baird, D.M., *Variation at the TERT locus and predisposition for cancer*. Expert Rev Mol Med, 2010. **12**: p. e16.
83. Venteicher, A.S., et al., *A human telomerase holoenzyme protein required for Cajal body localization and telomere synthesis*. Science, 2009. **323**(5914): p. 644-8.
84. Xiong, Y. and T.H. Eickbush, *Origin and evolution of retroelements based upon their reverse transcriptase sequences*. Embo j, 1990. **9**(10): p. 3353-62.
85. Cong, Y.S., J. Wen, and S. Bacchetti, *The human telomerase catalytic subunit hTERT: organization of the gene and characterization of the promoter*. Hum Mol Genet, 1999. **8**(1): p. 137-42.
86. Nakamura, T.M., et al., *Telomerase Catalytic Subunit Homologs from Fission Yeast and Human*. Science, 1997. **277**(5328): p. 955-959.
87. Wright, W.E., et al., *Telomerase activity in human germline and embryonic tissues and cells*. Dev Genet, 1996. **18**(2): p. 173-9.
88. Counter, C.M., et al., *Telomere shortening associated with chromosome instability is arrested in immortal cells which express telomerase activity*. Embo j, 1992. **11**(5): p. 1921-9.
89. Sharma, H.W., et al., *Differentiation of immortal cells inhibits telomerase activity*. Proc Natl Acad Sci U S A, 1995. **92**(26): p. 12343-6.
90. Bestilny, L.J., et al., *Selective inhibition of telomerase activity during terminal differentiation of immortal cell lines*. Cancer Res, 1996. **56**(16): p. 3796-802.
91. Savovsky, E., et al., *Down-regulation of telomerase activity is an early event in the differentiation of HL60 cells*. Biochem Biophys Res Commun, 1996. **226**(2): p. 329-34.
92. Shay, J.W. and W.E. Wright, *Role of telomeres and telomerase in cancer*. Semin Cancer Biol, 2011. **21**(6): p. 349-53.
93. Hanahan, D. and R.A. Weinberg, *The hallmarks of cancer*. Cell, 2000. **100**(1): p. 57-70.

94. Hanahan, D. and R.A. Weinberg, *Hallmarks of cancer: the next generation*. Cell, 2011. **144**(5): p. 646-74.
95. Kim, N.W., et al., *Specific association of human telomerase activity with immortal cells and cancer*. Science, 1994. **266**(5193): p. 2011-5.
96. Cong, Y.S., W.E. Wright, and J.W. Shay, *Human telomerase and its regulation*. Microbiol Mol Biol Rev, 2002. **66**(3): p. 407-25, table of contents.
97. Heaphy, C.M. and A.K. Meeker, *The potential utility of telomere-related markers for cancer diagnosis*. J Cell Mol Med, 2011. **15**(6): p. 1227-38.
98. Sommerfeld, H.J., et al., *Telomerase activity: a prevalent marker of malignant human prostate tissue*. Cancer Res, 1996. **56**(1): p. 218-22.
99. Koeneman, K.S., et al., *Telomerase activity, telomere length, and DNA ploidy in prostatic intraepithelial neoplasia (PIN)*. J Urol, 1998. **160**(4): p. 1533-9.
100. Meeker, A.K., *Telomeres and telomerase in prostatic intraepithelial neoplasia and prostate cancer biology*. Urol Oncol, 2006. **24**(2): p. 122-30.
101. Benetos, A., et al., *Short telomeres are associated with increased carotid atherosclerosis in hypertensive subjects*. Hypertension, 2004. **43**(2): p. 182-5.
102. Samani, N.J., et al., *Telomere shortening in atherosclerosis*. Lancet, 2001. **358**(9280): p. 472-3.
103. Valdes, A.M., et al., *Telomere length in leukocytes correlates with bone mineral density and is shorter in women with osteoporosis*. Osteoporos Int, 2007. **18**(9): p. 1203-10.
104. Epel, E.S., et al., *Accelerated telomere shortening in response to life stress*. Proc Natl Acad Sci U S A, 2004. **101**(49): p. 17312-5.
105. Valdes, A.M., et al., *Obesity, cigarette smoking, and telomere length in women*. Lancet, 2005. **366**(9486): p. 662-4.
106. Okuda, K., et al., *Telomere length in the newborn*. Pediatr Res, 2002. **52**(3): p. 377-81.
107. Youngren, K., et al., *Synchrony in telomere length of the human fetus*. Hum Genet, 1998. **102**(6): p. 640-3.
108. Baird, D.M., et al., *Telomere instability in the male germline*. Hum Mol Genet, 2006. **15**(1): p. 45-51.
109. Engelhardt, M., et al., *Relative contribution of normal and neoplastic cells determines telomerase activity and telomere length in primary cancers of the prostate, colon, and sarcoma*. Clin Cancer Res, 1997. **3**(10): p. 1849-57.
110. Meeker, A.K., et al., *Telomere shortening is an early somatic DNA alteration in human prostate tumorigenesis*. Cancer Res, 2002. **62**(22): p. 6405-9.
111. Vukovic, B., et al., *Evidence of multifocality of telomere erosion in high-grade prostatic intraepithelial neoplasia (HPIN) and concurrent carcinoma*. Oncogene, 2003. **22**(13): p. 1978-87.
112. Fernandez-Marcelo, T., et al., *Telomere length and telomerase activity in non-small cell lung cancer prognosis: clinical usefulness of a specific telomere status*. J Exp Clin Cancer Res, 2015. **34**: p. 78.
113. Svenson, U., B. Ljungberg, and G. Roos, *Telomere length in peripheral blood predicts survival in clear cell renal cell carcinoma*. Cancer Res, 2009. **69**(7): p. 2896-901.
114. McGrath, M., et al., *Telomere length, cigarette smoking, and bladder cancer risk in men and women*. Cancer Epidemiol Biomarkers Prev, 2007. **16**(4): p. 815-9.
115. Wu, X., et al., *Telomere dysfunction: a potential cancer predisposition factor*. J Natl Cancer Inst, 2003. **95**(16): p. 1211-8.
116. Mirabello, L., et al., *The association between leukocyte telomere length and cigarette smoking, dietary and physical variables, and risk of prostate cancer*. Aging Cell, 2009. **8**(4): p. 405-13.

117. Landi, M.T., et al., *A genome-wide association study of lung cancer identifies a region of chromosome 5p15 associated with risk for adenocarcinoma*. Am J Hum Genet, 2009. **85**(5): p. 679-91.
118. Shete, S., et al., *Genome-wide association study identifies five susceptibility loci for glioma*. Nat Genet, 2009. **41**(8): p. 899-904.
119. Petersen, G.M., et al., *A genome-wide association study identifies pancreatic cancer susceptibility loci on chromosomes 13q22.1, 1q32.1 and 5p15.33*. Nat Genet, 2010. **42**(3): p. 224-8.
120. Stacey, S.N., et al., *New common variants affecting susceptibility to basal cell carcinoma*. Nat Genet, 2009. **41**(8): p. 909-14.
121. Wang, L., et al., *Survival prediction in patients with glioblastoma multiforme by human telomerase genetic variation*. J Clin Oncol, 2006. **24**(10): p. 1627-32.
122. Jin, G., et al., *Dual roles of a variable number of tandem repeat polymorphism in the TERT gene in lung cancer*. Cancer Sci, 2011. **102**(1): p. 144-9.
123. Carpentier, C., et al., *Association of telomerase gene hTERT polymorphism and malignant gliomas*. J Neurooncol, 2007. **84**(3): p. 249-53.
124. Wang, L., et al., *A functional variant of tandem repeats in human telomerase gene was associated with survival of patients with early stages of non-small cell lung cancer*. Clin Cancer Res, 2010. **16**(14): p. 3779-85.
125. Andersson, U., et al., *MNS16A minisatellite genotypes in relation to risk of glioma and meningioma and to glioblastoma outcome*. Int J Cancer, 2009. **125**(4): p. 968-72.
126. Zhang, Y., et al., *A functional tandem-repeats polymorphism in the downstream of TERT is associated with the risk of nasopharyngeal carcinoma in Chinese population*. BMC Med, 2011. **9**: p. 106.
127. Wang, Y., et al., *A tandem repeat of human telomerase reverse transcriptase (hTERT) and risk of breast cancer development and metastasis in Chinese women*. Carcinogenesis, 2008. **29**(6): p. 1197-201.
128. American Type Culture Collection (ATCC). 2015 02.03.2015]; Available from: http://www.lgcstandards-atcc.org/?geo_country=at.
129. Nakamura, Y., K. Koyama, and M. Matsushima, *VNTR (variable number of tandem repeat) sequences as transcriptional, translational, or functional regulators*. J Hum Genet, 1998. **43**(3): p. 149-52.
130. Chinen, K., E. Takahashi, and Y. Nakamura, *Isolation and mapping of a human gene (SEC14L), partially homologous to yeast SEC14, that contains a variable number of tandem repeats (VNTR) site in its 3' untranslated region*. Cytogenet Cell Genet, 1996. **73**(3): p. 218-23.
131. Asghari, V., et al., *Dopamine D4 receptor repeat: analysis of different native and mutant forms of the human and rat genes*. Mol Pharmacol, 1994. **46**(2): p. 364-73.
132. Van Tol, H.H., et al., *Multiple dopamine D4 receptor variants in the human population*. Nature, 1992. **358**(6382): p. 149-52.
133. Tovar, D., J.C. Faye, and G. Favre, *Cloning of the human RHOB gene promoter: characterization of a VNTR sequence that affects transcriptional activity*. Genomics, 2003. **81**(5): p. 525-30.
134. Alakurtti, K., et al., *Characterization of the cystatin B gene promoter harboring the dodecamer repeat expanded in progressive myoclonus epilepsy, EPM1*. Gene, 2000. **242**(1-2): p. 65-73.
135. Lee, L.T., I.P. Lam, and B.K. Chow, *A functional variable number of tandem repeats is located at the 5' flanking region of the human secretin gene plays a downregulatory role in expression*. J Mol Neurosci, 2008. **36**(1-3): p. 125-31.
136. Iwashita, S., K. Koyama, and Y. Nakamura, *VNTR sequence on human chromosome 11p15 that affects transcriptional activity*. J Hum Genet, 2001. **46**(12): p. 717-21.

137. Durkop, H., et al., *Structure of the Hodgkin's lymphoma-associated human CD30 gene and the influence of a microsatellite region on its expression in CD30(+) cell lines*. Biochim Biophys Acta, 2001. **1519**(3): p. 185-91.
138. Chevalier, D., et al., *Characterization of new mutations in the coding sequence and 5'-untranslated region of the human prostacyclin synthase gene (CYP8A1)*. Hum Genet, 2001. **108**(2): p. 148-55.
139. Spire-Vayron de la Moureyre, C., et al., *Characterization of a variable number tandem repeat region in the thiopurine S-methyltransferase gene promoter*. Pharmacogenetics, 1999. **9**(2): p. 189-98.
140. Zheng, R. and G.A. Blobel, *GATA Transcription Factors and Cancer*. Genes Cancer, 2010. **1**(12): p. 1178-88.
141. Guo, M., et al., *Hypermethylation of the GATA genes in lung cancer*. Clin Cancer Res, 2004. **10**(23): p. 7917-24.
142. Akiyama, Y., et al., *GATA-4 and GATA-5 transcription factor genes and potential downstream antitumor target genes are epigenetically silenced in colorectal and gastric cancer*. Mol Cell Biol, 2003. **23**(23): p. 8429-39.
143. *Gene Expression Omnibus*. [Database] 31.03.2015]; Available from: <http://www.ncbi.nlm.nih.gov/geo/>.
144. Bild, A.H., et al., *Oncogenic pathway signatures in human cancers as a guide to targeted therapies*. Nature, 2006. **439**(7074): p. 353-7.
145. Wallace, T.A., et al., *Tumor immunobiological differences in prostate cancer between African-American and European-American men*. Cancer Res, 2008. **68**(3): p. 927-36.
146. *UniProt* 12.04.2015]; Available from: <http://www.uniprot.org/uniprot/?query=GATA+2&sort=score>.
147. *Addgene*. 24.11.2015]; Available from: <https://www.addgene.org/vector-database/>.

List of figures

Figure 1. hTERT gene organisation (Wang et al. 2003).	9
Figure 2. Promoter structure of hTERT antisense RNA (Wang et al. 2003).	9
Figure 3. Verifying MNS16A cloning, using restriction digestion and agarose gel electrophoresis.	28
Figure 4. Verifying purified MNS16A constructs, using restriction digestion and agarose gel electrophoresis.	29
Figure 5. Amount comparison to verify quantified DNA concentrations of the purified MNS16A constructs.	30
Figure 6. Verifying second round of purified MNS16A constructs, using restriction digestion and agarose gel electrophoresis.	31
Figure 7. pAdlox CFP transfection of lung cancer cell line A-427 for qualitative determination of transfection efficiency.	34
Figure 8. pAdlox CFP transfection of prostate cancer cell line LNCaP for qualitative determination of transfection efficiency.	35
Figure 9. Boxplot diagram of measured values from all six MNS16A VNTRs in the lung cancer cell line A-427.	37
Figure 10. Regression analysis of MNS16A VNTR promoter activities in A-427.	38
Figure 11. Boxplot diagram of measured values from all six MNS16A VNTRs in the prostate cancer cell line LNCaP.	39
Figure 12. Dotplot presentation of single MNS16A promoter activities in LNCaP.	40
Figure 13. Boxplot diagram of pGL3 normalized MNS16A VNTRs values of A-427 and LNCaP.	41
Figure 14. Sequences of the six different MNS16A alleles.	60

List of tables

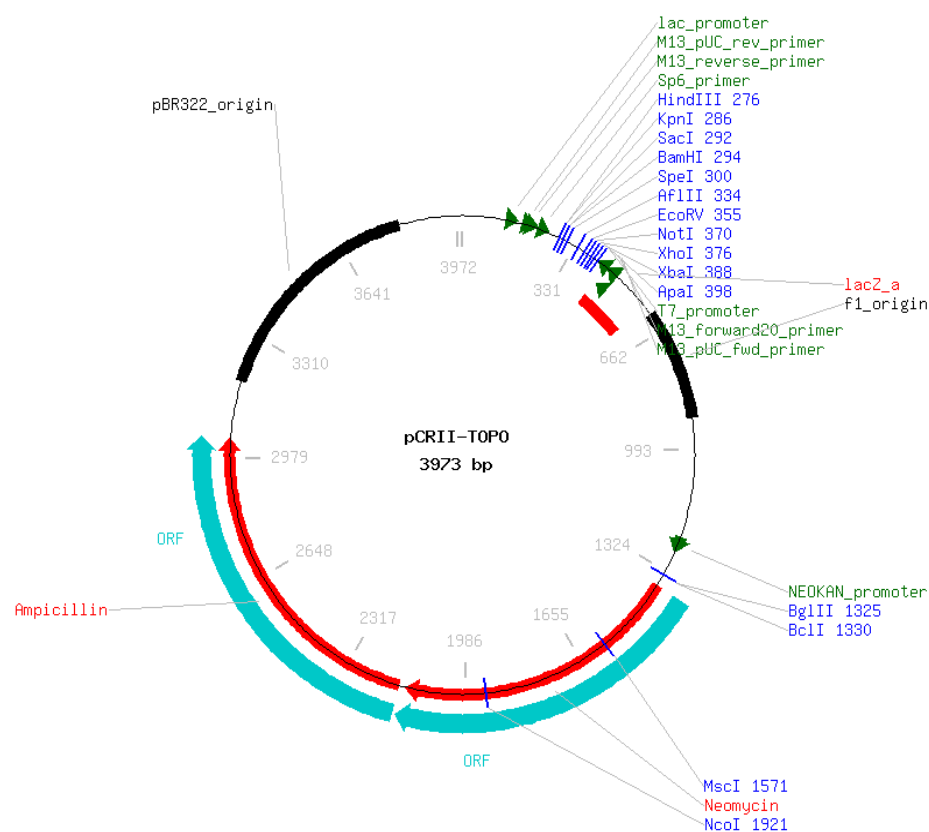
Table 1. All used plasmid vectors are listed.	12
Table 2. All used restriction digestions are listed.	12
Table 3. All used restriction digestions are listed.	12
Table 4. All used restriction enzymes are listed.	14
Table 5. Components of 1xTAE.	15
Table 6. Components of 6xloading buffer.	15
Table 7. Production of λ marker.	15
Table 8. Components of STETL buffer.	17
Table 9. Components of RNaseA.	17
Table 10. Components of LB Broth-medium.	18
Table 11. Restriction digestions after cesium chloride banding.	20
Table 12. Production of different solutions for cesium chloride banding.	20
Table 13. All used cancer cell lines.	21
Table 14. Production of different solutions used for cell cultivation.	22
Table 15. Eight different transfection approaches, used per cell line.	23
Table 16. Production of two different buffers for CFP transfection.	24
Table 17. Instrumental setting for measuring luciferase activities.	25
Table 18. MNS16A fragment lengths after cloning VNTRs from pCRII-TOPO vector.	27
Table 19. Quantified MNS16A DNA concentrations.	29
Table 20. Quantified MNS16A DNA concentrations.	30
Table 21. Quantified concentrations of cloned MNS16A preparations.	32
Table 22. Statistical results to determine promoter activity of MNS16A constructs in A-427.	37
Table 23. Statistical results to determine promoter activity of MNS16A constructs in LNCaP.	39
Table 24. Statistical results for comparing MNS16A promoter activity of both used cell lines.	41

Appendix 1: MNS16A allele sequences

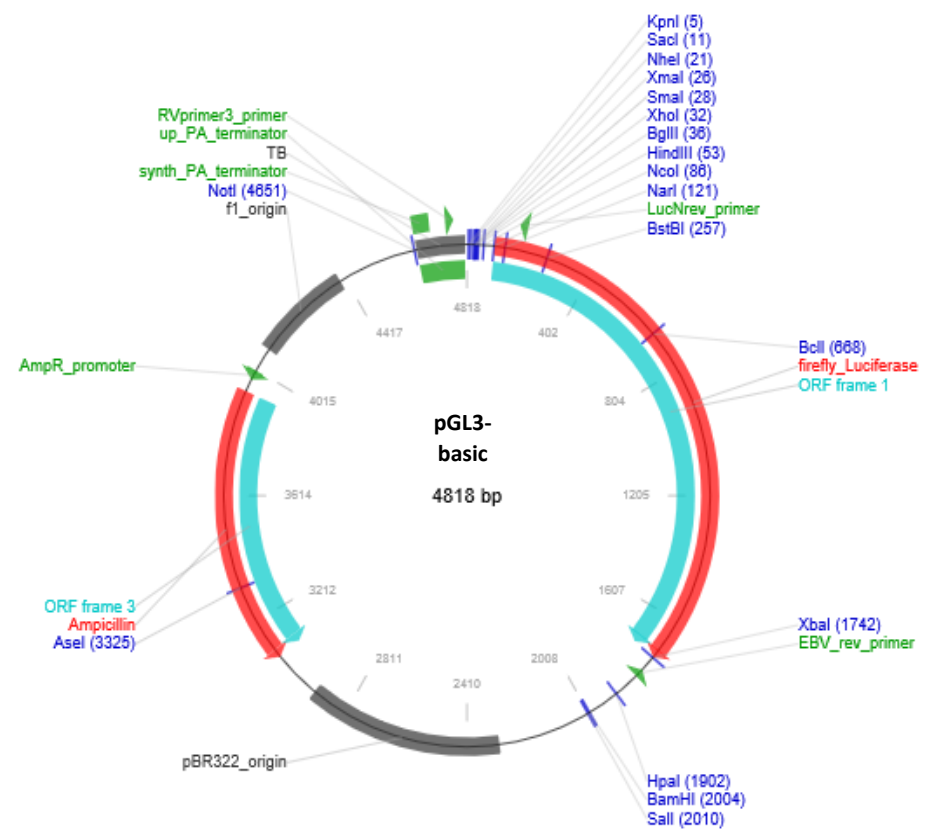
[illegible]

Figure 14. Sequences of the six different MNS16A alleles. CAT indicates the CAT trinucleotide insertion, whereas the asterisk indicates no CAT insertion. The core repeat elements are represented by boxes [2, 3].

Appendix 2: Vector maps

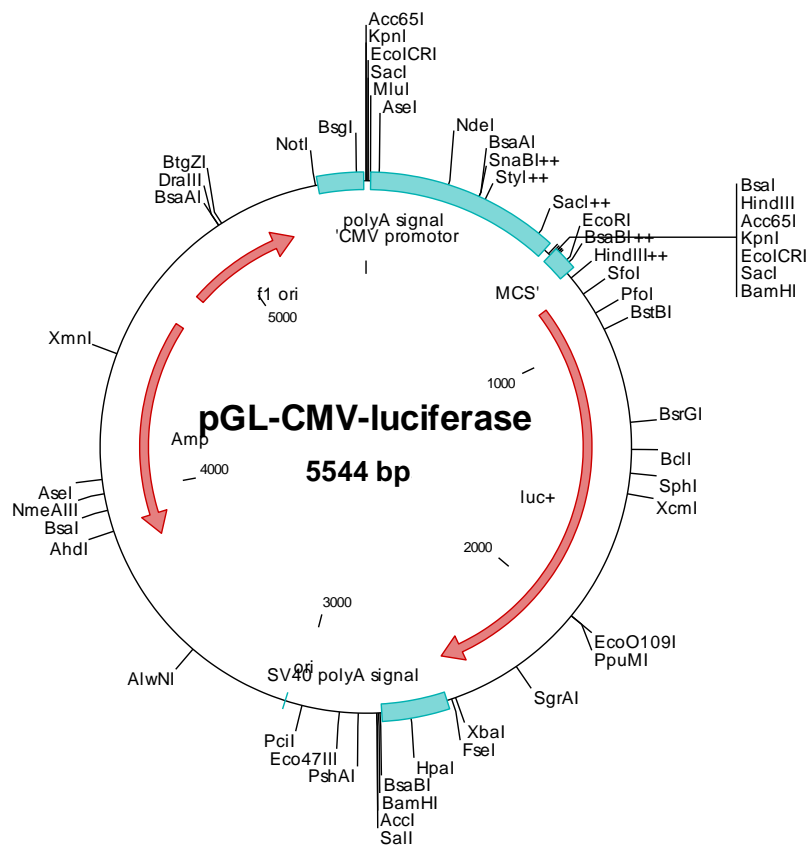
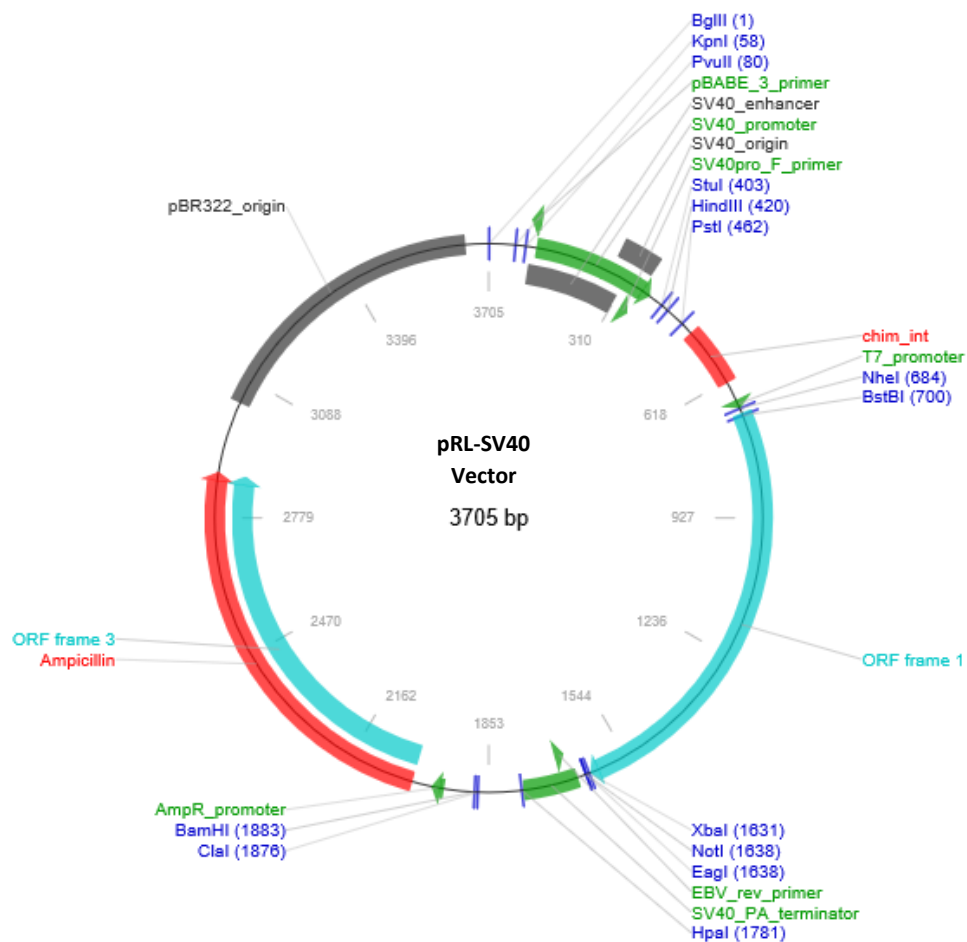


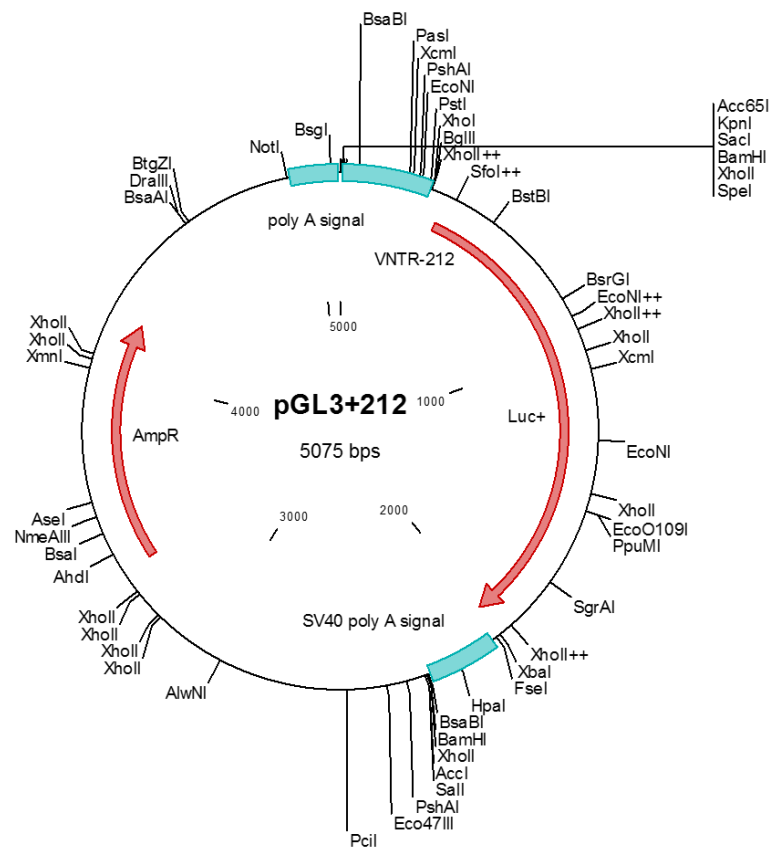
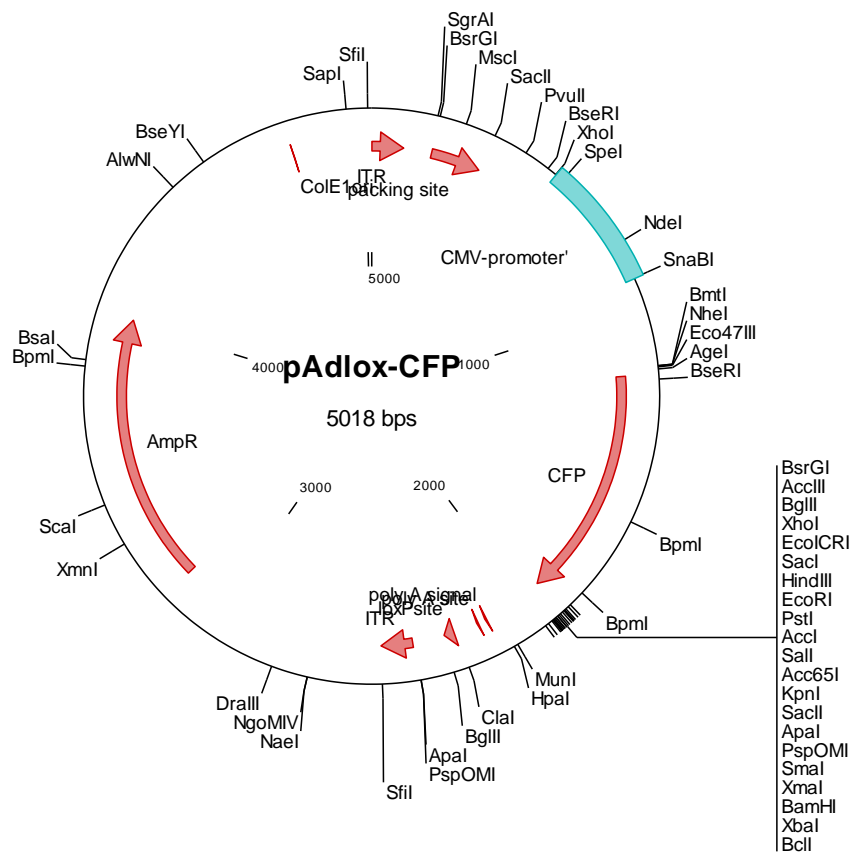
[147]

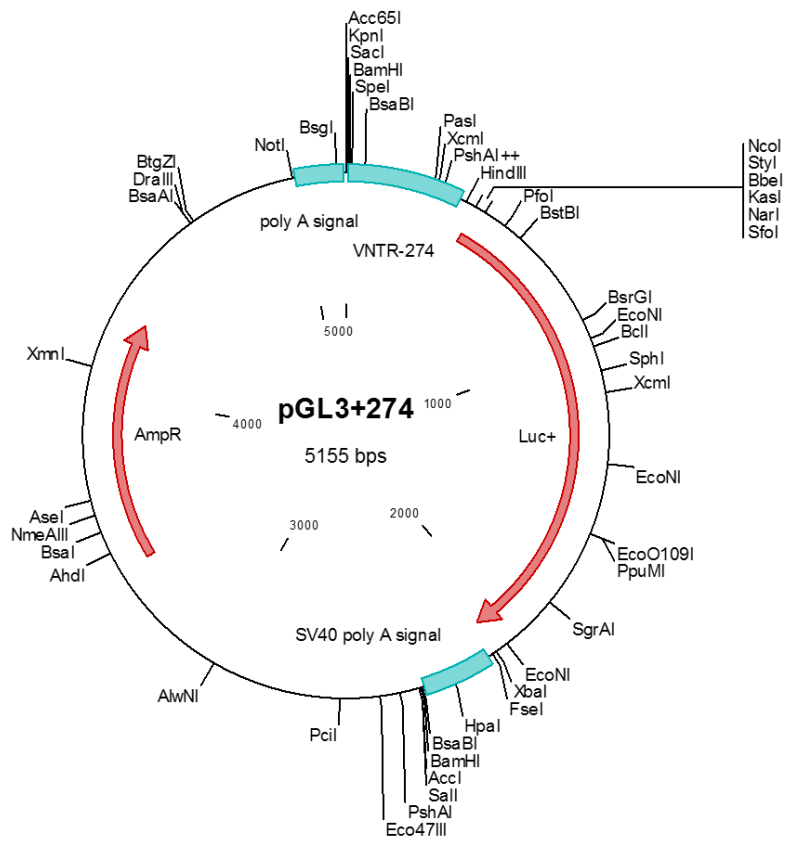
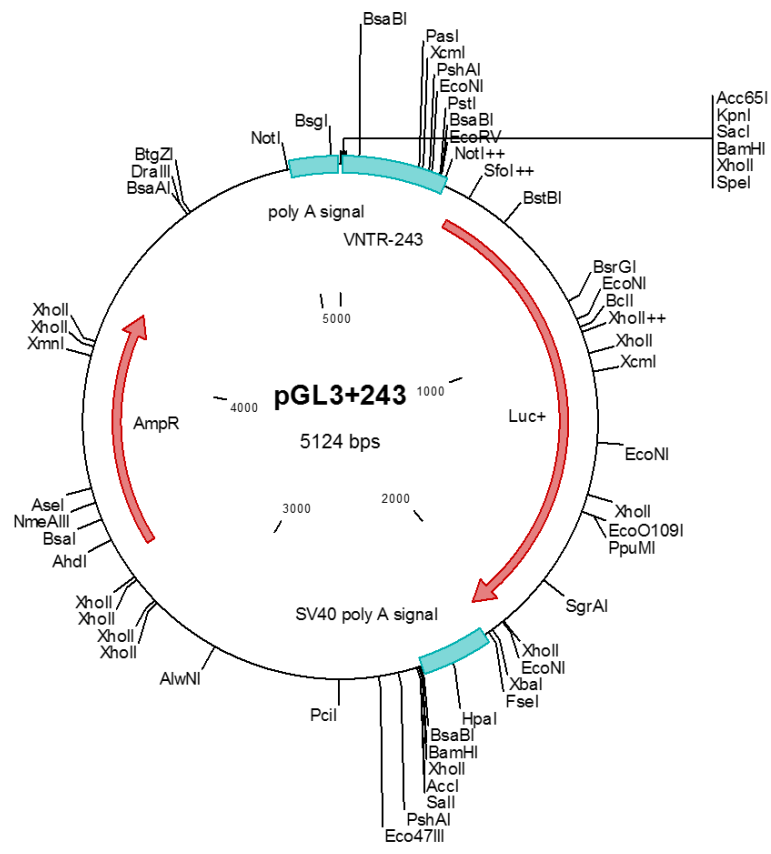


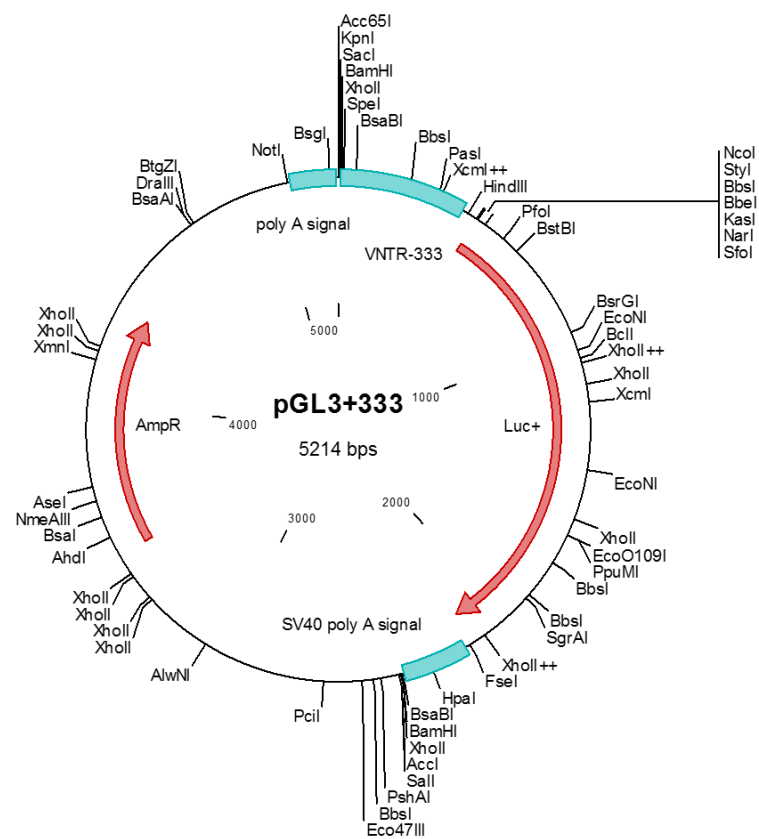
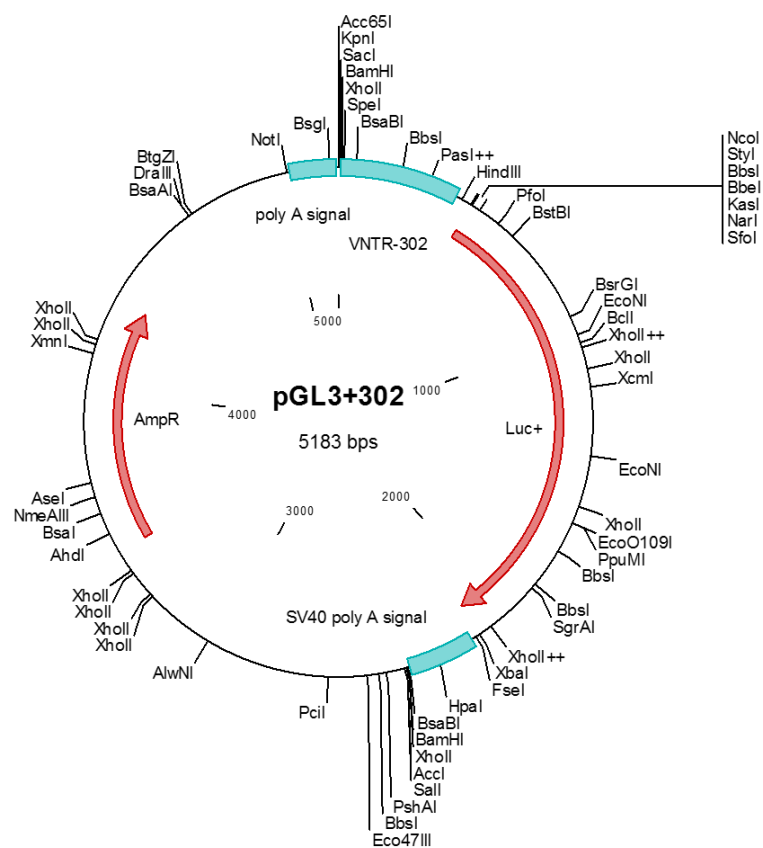
[147]

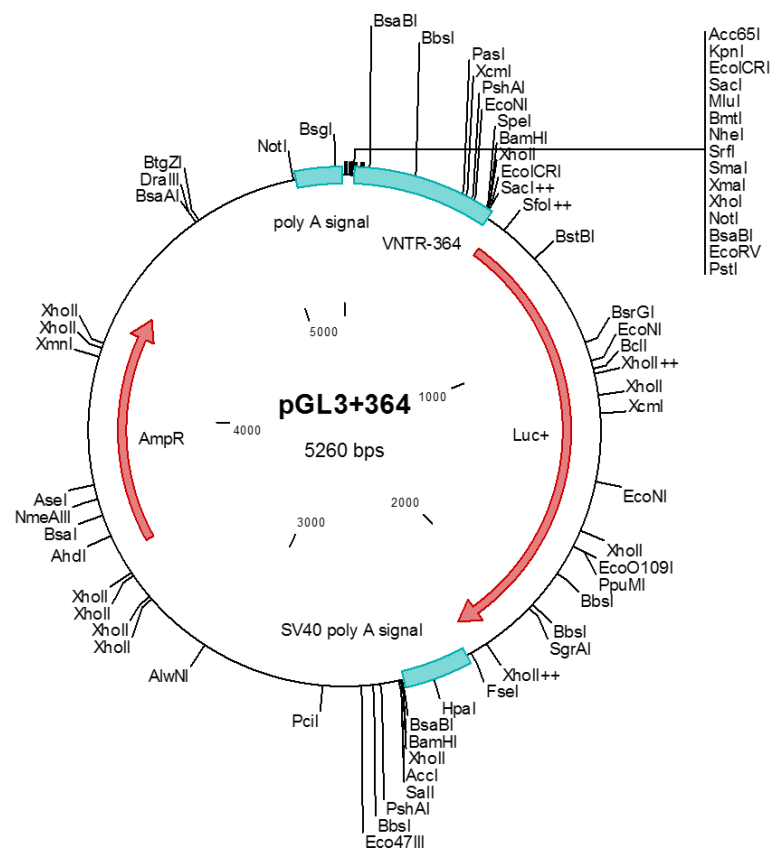
[147]











Appendix 3: Abstract

MNS16A, a polymorphic tandem repeats minisatellite in the promoter region of the antisense transcript of the human telomerase reverse transcriptase (hTERT) gene, has been discussed as a biomarker in several malignancies.

The present master thesis investigated, for the first time, the functionality of all six known MNS16A VNTRs in the lung cancer cell line A-427 and the prostate cancer cell line LNCaP, using a Dual-Luciferase reporter assay system.

All six MNS16A VNTRs showed statistically significant promoter activity in both cancer cell lines. LNCaP exhibited a statistically significant increase of promoter activity with decreasing MNS16A length for all six considered VNTRs, reflecting a strong negative linear relationship ($p=0.00078$) in the prostate cancer cell line. However, this trend was not observed in A-427. In A-427, VNTR-364, the longest allele, showed the lowest promoter activity, however no significant differences between the remaining five VNTRs were observed.

These results suggest that MNS16A functionality might differ in different cancer cell types and may not follow a linear function in all cell lines as observed in LNCaP. Further studies are warranted to investigate MNS16A functionality in additional prostate and lung cancer cell lines and in various other cancer cell lines.

Appendix 4: Kurzfassung

Der polymorphe Minisatellit MNS16A befindet sich downstream des humanen Telomerase Reverse Transcriptase (hTERT) Gens, in der Promoterregion des antisense hTERT Transkriptes. MNS16A wurde in zahlreichen molekular-epidemiologischen Studien als möglicher Biomarker für unterschiedliche Krebserkrankungen untersucht. Im Zuge dieser Studien wurden bisher sechs verschiedene Varianten mit einer variablen Anzahl an Tandemwiederholungen (VNTRs) von MNS16A identifiziert.

Ziel der vorliegenden Masterarbeit war, zum ersten Mal, der Funktionalitätsnachweis aller sechs bekannten MNS16A Varianten, nicht nur in der Lungenkrebs-Zelllinie A-427, sondern auch in der Prostatakrebs-Zelllinie LNCaP, unter Verwendung eines Dual-Luciferase Reporter Systems.

Alle sechs MNS16A VNTRs zeigten eine statistisch signifikante Promoteraktivität in beiden Krebszelllinien. In der Prostatakrebs-Zelllinie zeigte sich eine statistisch signifikante Zunahme der Promoteraktivität mit abnehmender MNS16A Länge. Dies deutet auf ein starkes negatives lineares Verhältnis ($p=0.00078$) in der Prostatakrebs-Zelllinie hin. Allerdings konnte dieses Verhältnis in die Lungenkrebs-Zelllinie A-427 nicht bestätigt werden. Obwohl in A-427 das längste Allel eine deutlich geringere Promoteraktivität aufweist als die übrigen MNS16A Varianten, gelang es nicht, einen statistisch signifikanten Unterschied in der Aktivität der kürzeren Allele nachzuweisen.

Diese Resultate weisen auf ein unterschiedliches Verhalten von MNS16A in unterschiedlichen Krebszellen hin. Weitere Studien, die die MNS16A Funktionalität in zusätzlichen Lungen- und Prostatakrebs-Zelllinien und in anderen Krebszelllinien untersuchen, können zur weiteren Aufklärung der MNS16A Funktionalität beitragen.

Curriculum Vitae

Name: Christian Behm, BSc
Gender: Male
Date of Birth: 22nd of June, 1990
Place of Birth: Güssing, Burgenland
Nationality: Austria

Education

1996 – 2000 Volksschule Moschendorf
2000 – 2004 Hauptschule Eberau
2004 – 2008 Bundesoberstufenrealgymnasium Güssing with focus on natural science
2009 – 2013 University of Vienna to receive bachelor's degree in Biology, with focus on Molecular Biology
Since 2013 University of Vienna to receive master's degree in Molecular Biology, with focus on Molecular Medicine

Working experience

April – June 2012 **Internship to receive bachelor's degree**, Department of Biochemistry and Cell Biology, Max F. Perutz Laboratories, University of Vienna, Univ.-Prof. Dr. Friedrich Propst
August 2012 **Internship at the Institut of Cancer Research**, Department of Internal Medicine 1, Medical University of Vienna, Ao. Prof. Mag. Dr. Andrea Gsur
May 2013 – February 2014 **Master's Thesis at the Insitut of Cancer Research**, Department of Internal Medicine 1, Medical University of Vienna, Ao. Prof. Mag. Dr. Andrea Gsur
August 2014 **Internship at the Department of Medicine 1**, Devision of Hematology and Hemostaseology, Medical University of Vienna, Ass. Prof. Katrina Vanura, PhD
November – December 2014 **Internship at the Department of Molecular Cell Biology**, Max F. Perutz Laboratories, Medical University of Vienna, Ao. Univ.-Prof. Dr. Egon Ogris